Title
THE ELECTRONIC STRUCTURE OF TRIGONAL AND AMORPHOUS Se AND Te

Authors
Joannopoulos, J.D.
Schluter, M.
Cohen, Marvin L.

Publication Date
1974-08-01

Submitted to Physical Review

LBL-3130
Preprint c.2(Rpl.)

THE ELECTRONIC STRUCTURE OF TRIGONAL AND AMORPHOUS Se AND Te

J. D. Joannopoulos, M. Schlüter and Marvin L. Cohen

August, 1974

Prepared for the U. S. Atomic Energy Commission
under Contract W-7405-ENG-48

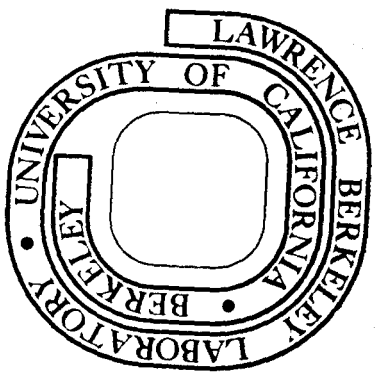

DISCLAIMER

The Electronic Structure of Trigonal and Amorphous Se and Te*

J. D. Joannopoulos,† M. Schlüter‡ and Marvin L. Cohen
Department of Physics, University of California and
Inorganic Materials Research Division,
Lawrence Berkeley Laboratory, Berkeley, California 94720

Abstract

The electronic structure of trigonal and amorphous Se and Te is investigated using the empirical pseudopotential method (EPM), charge density calculations and simple tight binding models. Band structures and electronic densities of states are obtained which are in excellent agreement with recent photoemission measurements. The tight binding models are used to obtain analytic expressions for the energy bands and to interpret the EPM band structures in terms of real space orbital-orbital interactions. Charge density calculations obtained as a function of energy and evaluated within specific energy intervals are used to interpret various structure in the density of states. Specifically certain easily resolvable peaks in the experimental photoemission spectra are associated with intra-chain and inter-chain localized states respectively. By taking only short wavelength components of the charge density,

a bonding charge can be defined which gives an estimate of the intra- vs inter-chain bonding strengths. The trigonal results along with model calculations to investigate the effects of bond angle variations on chains and the presence of eight and six-fold rings of bonds are used to interpret the changes observed in the experimental spectra of amorphous Se and Te. A new model of amorphous Se is proposed.

I. Introduction

To gain a good understanding of the electronic structure of any system it is important to study the electronic density of states of this system. The main reasons for this are that the density of states contains information which is easily accessible and (1) remains a well defined quantity regardless of structure, (2) is sensitive to effects of periodicity, (3) contains basic information about the bonding nature of the system, (4) is sensitive to the topology of the system, and (5) reflects the intrinsic atomic nature of the systems constituents.

A thorough study of the electronic density of states should involve a realistic calculation to facilitate comparisons with experiment, a careful examination of the calculated spectra (e.g. in terms of charge distributions) and simple model calculations which can aid in interpreting main features in a simple physical way. Experimentally, information about

the density of states can be obtained from ultraviolet (UPS) and X-ray (XPS) photoemission measurements as well as X-ray emission and absorption experiments. The trigonal and amorphous phases of Se and Te are excellent systems for the study described above since new UPS[1] and XPS[1-3] measurements have provided important information about all the valence bands and have revealed many inadequacies of current theoretical calculations.[4-7] In one of these calculations[4] a complete merging of the s- and p-like bands was proposed; this disagrees qualitatively with the recent photoemission data. Other calculations[5-7] show a separation of s- and p-like bands which is in qualitative agreement with photoemission experiments, however band widths and important structure are not correct. In addition, no calculations exist giving a detailed analysis of the electronic nature of structure in the density of states. The photoemission measurements also show some remarkable differences between the trigonal and amorphous phases. One of these differences corresponds to a seemingly <u>sharper</u> structure in the s-like region of the density of states of the <u>amorphous phase</u>. This is quite an unusual behavior for an amorphous spectrum. Other important differences between amorphous and crystalline data appear when comparing the intensities of the two peaks of the bonding p-like region of the density of states. To understand and interpret these differences it is first necessary to have a good understanding of the origin of the structure in the trigonal spectra.

We thus present in this paper new calculations of the band structure, densities of states and charge densities for trigonal Se and Te using the empirical pseudopotential method (EPM).[8] We also introduce simple tight binding models described by a set of parameters which are related to important physical interactions in the system. In addition we have calculated the densities of states for various model structures as an aid in interpreting the amorphous photoemission results.

The format of the paper is as follows. In Section II we discuss the structural aspects of Se and Te. In Section III we discuss the method and parameters used in our EPM calculations and we introduce and discuss two tight binding models. In Section IV we present the results of our calculations for trigonal Se and Te using the EPM and tight binding models and give a new interpretation of the photoemission spectra. In Section V we present our model calculations and we discuss and interpret the amorphous spectra. Finally in Section VI we make some concluding remarks.

II. Structural Considerations

The crystal structure of trigonal Se and Te consists of helical chains which spiral around axes parallel to the crystalline c-axis. The helices are arranged in an hexagonal array. The crystal unit cell consists of three atoms of one helix and is shown in Fig. 1(a). The space groups of trigonal Se and Te are D_3^4 or D_3^6 depending on the sense of rotation

of the helical chains. The existence of chains is manifested by the fact that each atom is tightly covalently bonded to two neighbors as one would expect for elements with six valence electrons.[9] The bonding between individual chains is much weaker and is often believed to be of van der Waals character. We shall however show in this paper that there is definitely some covalent-like bonding between neighboring chains. The anisotropy-ratio of intra-chain bonding strength versus inter-chain bonding strength decreases in going from Se to Te. This is reflected in their mechanical properties[10] and in the ratio of inter-chain versus intra-chain atomic distances d_2/d_1 = 1.49 for Se and 1.31 for Te. In fact the next heavier group VI element Po crystallizes in an isotropic simple cubic structure into which Te and Se transform under hydrostatic pressures of about 60 kbar and about 130 kbar respectively.[10] The close relationship between the trigonal structure of Se and Te and the simple cubic structure can be recognized by comparing Fig.s 1(a) and 1(b). A rough picture of the electronic structure of Se and Te can be obtained by considering the strong intra-chain bonding only. Since the atomic s-states are well separated from the higher p-states (~10 eV for Se and ~8 eV for Te) it is expected that s-p mixing will be small in the crystal. This does not at all contradict a bond angle of about 104° if one allows for slight mixing with d-states as well. In fact we obtained from our pseudopotential calculations by angular projection about

5-10% s- and 1-5% d-admixture to the bonding p-states. The deep-lying s-states overlap on neighboring atoms and combine into bonding- and anti-bonding like states. Since there is only one s-state per atom available, two complete covalent bonds per atom cannot be accomplished this way. As in a metal there will be no gap between these s-states and since all states are fully occupied the net contribution of the s-states to the cohesive energy will be small. The two bonds per atom are thus essentially formed by p-states with small admixtures of s- and d-character. This leaves one non-bonding p-state per atom. The six electrons per atom therefore occupy the s-states, the bonding p-like states and the non-bonding or lone-pair states. The Fermi level falls between the non-bonding and the anti-bonding p-like states.

III. Calculational Methods

A. EPM and Bonding Charge Model

The EPM has been previously discussed extensively.[8] Briefly the method involves solving a secular equation for the pseudopotential Hamiltonian which has the form:

$$H = -\frac{\hbar^2}{2m}\nabla^2 + V(\underset{\sim}{r}) \qquad (1)$$

Using crystal symmetry the weak pseudopotential $V(\underset{\sim}{r})$ is expanded in the reciprocal lattice.

$$V(\underset{\sim}{r}) = \sum_{\underset{\sim}{G}} V(\underset{\sim}{G}) e^{i\underset{\sim}{G}\cdot\underset{\sim}{r}} \qquad (2)$$

where $\underset{\sim}{G}$ is a reciprocal lattice vector. For the case of

one type of atom $V(\underset{\sim}{G})$ can be written

$$V(\underset{\sim}{G}) = V_f(|\underset{\sim}{G}|)S(\underset{\sim}{G}) \tag{3}$$

where $S(\underset{\sim}{G})$ is the structure factor and $V_f(|\underset{\sim}{G}|)$ is a form factor of the atomic pseudopotential. $S(\underset{\sim}{G})$ and $V_f(|\underset{\sim}{G}|)$ are given by

$$S(\underset{\sim}{G}) = \frac{1}{n} \sum_i e^{-i\underset{\sim}{G}\cdot\underset{\sim}{\tau}_i} \tag{4}$$

$$V_f(|\underset{\sim}{G}|) = \frac{n}{\Omega} \int V_a(|\underset{\sim}{r}|)e^{-i\underset{\sim}{G}\cdot\underset{\sim}{r}} d^3\underset{\sim}{r} \tag{5}$$

where n is the number of atoms per primitive cell, $\underset{\sim}{\tau}_i$ is the position of the i'th atom in the primitive cell, Ω, is the volume of the primitive cell and $V_a(|\underset{\sim}{r}|)$ is the atomic pseudopotential, assumed spherical. The values of $V_f(|\underset{\sim}{G}|)$ used in our calculations were obtained by fitting peaks in the density of states to the structure in experimental photoemission spectra.[1,2] To obtain good convergence we used about 60 plane waves as a basis set with an additional 300 plane waves through a perturbation technique developed by Löwdin.[11] We calculated $E(\underset{\sim}{k})$ in 1/12 of the Brillouin zone at 300 grid points. The density of states was then obtained using

$$N(E) = \frac{1}{NN_a} \sum_n \sum_{\underset{\sim}{k}} \delta(E-E_n(\underset{\sim}{k})) \tag{6}$$

where N_a is the number of atoms in the primitive cell, N is the number of primitive cells, and N(E) is normalized to the

number of states per atom. The method of Gilat and Raubenheimer[12] is used to evaluate the integral in Eq. (6). The energy derivatives required by this method were obtained using $\underset{\sim}{k}\cdot\underset{\sim}{p}$ perturbation theory.

Once we have the energies $E_n(\underset{\sim}{k})$ and the pseudo-wavefunctions $\phi_{n,\underset{\sim}{k}}(\underset{\sim}{r})$ for each band n, we can define an average "energy" charge density $\rho_E(\underset{\sim}{r})$ by

$$\rho_E(\underset{\sim}{r}) = e \sum_n \sum_{\underset{\sim}{k}} \delta(E_n(\underset{\sim}{k})-E)\left|\phi_{n,\underset{\sim}{k}}(\underset{\sim}{r})\right|^2 \qquad (7)$$

This can then be used to define $\rho_{E_f,E_i}(\underset{\sim}{r})$ for an interval $[E_i,E_f]$ by

$$\rho_{E_f,E_i}(\underset{\sim}{r}) = \int_{E_i}^{E_f} \rho_E(\underset{\sim}{r})dE \ . \qquad (8)$$

ρ_{E_f,E_i} is a very useful quantity for studying the distribution and character of the electrons in various regions $[E_i,E_f]$ of the density of states. Since $\rho_{E_f,E_i}(\underset{\sim}{r})$ is periodic, we can expand it as

$$\rho_{E_f,E_i}(\underset{\sim}{r}) = \sum_G \hat{\rho}_{E_f,E_i}(\underset{\sim}{G})e^{i\underset{\sim}{G}\cdot\underset{\sim}{r}} \qquad (9)$$

We can now go a step further and isolate the short wavelength Fourier components from the long wavelength Fourier components

$$\rho_{E_f,E_i}(\underset{\sim}{r}) = \rho^L_{E_f,E_i}(\underset{\sim}{r}) + \rho^S_{E_f,E_i}(\underset{\sim}{r}) \qquad (10)$$

with

$$\rho^S_{E_f,E_i}(\underset{\sim}{r}) \equiv \sum_{\underset{\sim}{G} \geq \frac{2\pi}{\lambda_0}} \hat{\rho}_{E_f,E_i}(\underset{\sim}{G})e^{i\underset{\sim}{G}\cdot\underset{\sim}{r}} \qquad (11a)$$

$$\rho^{L}_{E_f,E_i}(\underset{\sim}{r}) \equiv \sum_{\underset{\sim}{G}<\frac{2\pi}{\lambda_0}} \hat{\rho}_{E_f,E_i}(\underset{\sim}{G}) e^{i\underset{\sim}{G}\cdot\underset{\sim}{r}} \qquad (11b)$$

This introduces a new method of defining bonding charges and a way to separate out the effects of metallicity. The cutoff or boundary wavelength λ_0 between short and long wavelength components was found to lie naturally at $\lambda_0 = d$ where d is the nearest neighbor separation in Se or Te.

B. Tight Binding Model with Only Intra-chain Interactions

We now introduce a very simple tight binding model in which we include only intra-chain interactions. This model can be solved analytically and it contains the basic information for understanding the EPM band structures and the importance of a single chain as a unit. This model is particularly applicable to Se which is more anisotropic than Te. In the next section we will also include inter-chain interactions so that the extended model will be applicable to both Se and Te.

We begin by assigning to each atom a basis set consisting of an s-like orbital $|s\rangle$, two hybrid and mixed p-like orbitals $|p\rangle$, and one lone-pair $|\ell\rangle$ function. These orbitals are shown schematically in Fig. 2(a). The $|s\rangle$ orbitals constitute wavefunctions which are localized on the atoms and are essentially the atomic s-states of Se or Te. The $|p\rangle$ orbitals are primarily of atomic p nature, but also contain some s and d admixture. They are primarily concentrated along the bonds in the chain with small lobes at antibonding

sites. Finally the lone pair $|\ell>$ orbitals are taken to be pure atomic p-functions. We can now write down a Hamiltonian for the chain which is essentially "one-dimensional" and has the form

$$H = \sum_{i,i'} V_S^{i,i'} |s_i><s_{i'}| + \sum_{\substack{i,i' \\ j,j'}} V_p^{i,j,i',j'} |p_{i,j}><p_{i',j'}|$$

$$+ \sum_{i,j'} V_\ell^{i,i'} |\ell_i><\ell_{i'}| \qquad (12)$$

where i (or i') represents a particular atom and j(or j') = 1,2 is a particular bond of this atom. The first, second and third terms contain interactions among the s-orbitals, p-hybrid and mixed orbitals and lone-pair orbitals respectively. We neglect any other types of interactions. This is not a bad approximation and leaves us with a Hamiltonian that is decoupled and easy to work with. The interactions $V_s^{i,i'}$, $V_p^{i,j,i',j'}$ and $V_\ell^{i,i'}$ that we have chosen are shown in Fig. 2(b) and have physical interpretations that are easily understood. For $V_S^{i,i'}$ we take

$$V_s^{i,i'} = V_s \delta_{i,i'} + V_s'(1-\delta_{i,i'}) \qquad (13)$$

where V_s represents the position of the center of mass of the s-like band or essentially the atomic s-level. V_s' is the interaction between first nearest neighbors and is related to the width of this band. Next for $V_p^{i,j,i',j'}$ we take

$$V_p^{i,j,i',j'} = V_p \delta_{i,i'}\delta_{j,j'} + V_p' \delta_{i,i'}(1-\delta_{j,j'})$$

$$+ V_p'' \delta_{j,j'}(1-\delta_{i,i'}) + V_p'''(1-\delta_{j,j'})(1-\delta_{i,i'}) \qquad (14)$$

where V_p represents the center of mass energy of the p-like states and lies near the atomic p-level. V_p' represents the interaction of different $|p>$ orbitals on the same atom, V_p'' represents the interaction between hybrid orbitals on different atoms but along the same bond ($j = j'$) and V_p''' represents the interaction between hybrid orbitals on different atoms but <u>not</u> along the same bond ($j \neq j'$). V_p'' is also responsible for the bonding-antibonding splitting of the p-like states about V_p. Finally for $V_\ell^{i,i'}$ we take

$$V_\ell^{i,i'} = V_\ell \delta_{i,i'} + I_\ell^{i,i'}(1-\delta_{i,i'}) \qquad (15)$$

where V_ℓ is the center of mass position in energy of the lone-pair states and is taken to be different from V_p because of the hybridization of $|p>$. $I_\ell^{i,i'}$ represents first nearest neighbor interactions V_ℓ' and second nearest neighbor interactions V_ℓ''. The reasons for including second nearest neighbors in both $V_\ell^{i,i'}$ and $V_p^{i,j,i',j'}$ will be discussed later.

The trigonal structure contains only three atoms in a primitive cell so that the eigenvalues and density of states of this Hamiltonian can be obtained analytically quite easily. In particular the eigenvalues of the hybrid and mixed p-like part of the Hamiltonian can be related by an analytic transformation to the eigenvalues of a much simpler Hamiltonian in which we place only one localized state on an atom and take only nearest neighbor interactions into account. To show this, consider the chain shown in Fig. 3(a). For any

given atom i, we label the coefficients of the $|p>$ orbitals in the total wavefunction near this atom by a, b, c etc. For any a_j and b_j (where j = 1 or 2) Schroedinger's equation reduces to

$$Ea_j = (a_1+a_2)V_p' + b_jV_p'' + (c_j+b_k)V_p''' \qquad (16)$$

$$Eb_j = (b_j+c_j)V_p' + a_jV_p'' + (a_k+d_j)V_p''' \qquad (17)$$

where $j \neq k$ and we have assumed that $V_p = V_p'$ for convenience. If we now sum over k and j we get

$$2E\alpha_i = 4V_p'\alpha_i + 2V_p''\beta_i + 2V_p''' \sum_j \alpha_j \qquad (18)$$

$$2E\beta_i = 2V_p' \sum_j \alpha_j + 2V_p''\alpha_i + 2V_p''' \sum_j \beta_j \qquad (19)$$

where α_i is the sum of the coefficients of $|p>$ associated with atom i and β_i is the sum of the coefficients of $|p>$ associated with the first nearest neighbor atoms of atom i which lie along the bond pointing towards atom i. Thus in Fig. 3(a), $\alpha_i = a_1+a_2$ and $\beta_i = b_1+b_2$. Equations (18) and (19) can of course be written in terms of a matrix equation of the form

$$\begin{pmatrix} E-2V_p' & -V_p'' \\ -V_p'' & E \end{pmatrix} \begin{pmatrix} \alpha_i \\ \beta_i \end{pmatrix} = \begin{pmatrix} V_p''' & 0 \\ V_p' & V_p''' \end{pmatrix} \begin{pmatrix} \sum_j \alpha_j \\ \sum_j \beta_j \end{pmatrix} \qquad (20$$

Equation (20) can now be reduced to an equation of the form

$$\begin{pmatrix} \epsilon & 0 \\ 0 & \epsilon \end{pmatrix} \begin{pmatrix} \hat{\alpha}_i \\ \hat{\beta}_i \end{pmatrix} = \begin{pmatrix} V & 0 \\ 0 & V \end{pmatrix} \begin{pmatrix} \sum_j \hat{\alpha}_j \\ \sum_j \hat{\beta}_j \end{pmatrix} \qquad (21)$$

where $\hat{\alpha}_i$ and $\hat{\beta}_i$ are related by a unitary transformation to α_i and β_i and

$$E = V_p + V_p'' \varepsilon/V \pm \sqrt{(V_p')^2+(V_p'')^2+V_p'V_p''\varepsilon/V} \qquad (22)$$

where we have taken into account again the difference between V_p and V_p'. Thus the problem of solving the hybrid and mixed p-like part of H in equation (12) is reduced to solving the simple system described by

$$\varepsilon\hat{\alpha}_i = V \sum_j \hat{\alpha}_j \qquad (23)$$

whose eigenvalues are easily obtained and related to E by equation (22). This is similar to the one band-two band transformation used by Thorpe and Weaire[13] in the case of tetrahedrally coordinated solids. Using (12), (13), (23) and (22) we obtain for the trigonal case from $0 \leq k \leq \pi/c$ or Γ to A

$$E_1^s = V_s + 2V_s' \cos(\frac{kc}{3})$$

$$E_2^s = V_s + 2V_s' \cos(\frac{kc-2\pi}{3})$$

$$E_3^s = V_s + 2V_s' \cos(\frac{kc+2\pi}{3}) \qquad (24)$$

$$E_1^{pb} = V_p+2V_p''\cos(\frac{kc+2\pi}{3})-[(V_p')^2+(V_p'')^2+2V_p'V_p''\cos(\frac{kc+2\pi}{3})]^{1/2}$$

$$E_2^{pb} = V_p+2V_p''\cos(\frac{kc-2\pi}{3})-[(V_p')^2+(V_p'')^2+2V_p'V_p''\cos(\frac{kc-2\pi}{3})]^{1/2}$$

$$E_3^{pb} = V_p+2V_p''\cos(\frac{kc}{3})-[(V_p')^2+(V_p'')^2+2V_p'V_p''\cos(\frac{kc}{3})]^{1/2} \qquad (25)$$

$$E_1^{\ell} = V_{\ell}+2V_{\ell}'\cos(\frac{kc}{3})+2V_{\ell}''\cos(\frac{2kc}{3})$$

$$E_2^{\ell} = V_{\ell}+2V_{\ell}'\cos(\frac{kc-2\pi}{3})+2V_{\ell}''\cos(\frac{2kc+2\pi}{3})$$

$$E_3^{\ell} = V_{\ell}+2V_{\ell}'\cos(\frac{kc+2\pi}{3})+2V_{\ell}''\cos(\frac{2kc-2\pi}{3}) \qquad (26)$$

$$E_1^{pa} = V_p+2V_p'''\cos(\frac{kc}{3})+[(V_p')^2+(V_p'')^2+2V_p'V_p''\cos(\frac{kc}{3})]^{1/2}$$

$$E_2^{pa} = V_p+2V_p'''\cos(\frac{kc-2\pi}{3})+[(V_p')^2+(V_p'')^2+2V_p'V_p''\cos(\frac{kc-2\pi}{3})]^{1/2}$$

$$E_3^{pa} = V_p+2V_p'''\cos(\frac{kc+2\pi}{3})+[(V_p')^2+(V_p'')^2+2V_p'V_p''\cos(\frac{kc+2\pi}{3})]^{1/2} \qquad (27)$$

where E^s, E^{pb}, E^{ℓ} and E^{pa} represent the s-like, p-bonding-like, lone pair and p-antibonding-like bands respectively. The densities of states for these bands are given by

$$D_s(E) = \frac{3}{c} \cdot \frac{1}{[4(V_s')^2-(E-V_s)^2]^{1/2}} \qquad (28)$$

$$D_p(E) = \frac{3}{c} \frac{1}{[1-\Delta^2]^{1/2}} \left(\frac{2V_p'''\Delta-(E-V_p)}{2EV_p'''-4(V_p''')^2\Delta-V_p'V_p''}\right) \qquad (29)$$

$$D_{\ell}(E) = \frac{3}{2c} \frac{1}{[(1-\Lambda^2)(V'+4V''\Lambda)^2]} \qquad (30)$$

where

$$\Delta = \frac{2(E-V_p)V_p'''-V_p'V_p''}{4(V_p''')^2}$$

$$+ \frac{[4(V_p''')^2((V_p')^2+(V_p'')^2)-4(E-V_p)V_p'''V_p''V_p'+(V_p')^2(V_p'')^2]^{1/2}}{4(V_p''')^2} \qquad (31)$$

$$\Lambda = \frac{-V_\ell' + [(V_\ell')^2 + 8(V_\ell'')^2 + 4(E-V_\ell)V_\ell'']^{1/2}}{4V_\ell''} \qquad (32)$$

C. Tight Binding Model Including Inter-chain Interactions

A three dimensional view of the trigonal structure is shown in Fig. 1(a). As we have already mentioned the trigonal structure can be changed to a simple cubic structure (Fig. 1(b)) with just a small trigonal distortion. This is very convenient since it provides a very simple way of choosing the most important tight-binding parameters to use in a "three-dimensional" model. The method we will use in selecting a set of tight binding parameters is the following. We consider the simple cubic structure and obtain all the interactions between nearest neighbor atoms. We explicitly retain the identity of the individual chains and hence the character of the tight binding orbitals $|s\rangle$, $|p\rangle$ and $|\ell\rangle$ as in Section IIIB. In this way each interaction can be classified as an inter-chain or intra-chain interaction. For example for the $|s\rangle$ orbitals we have six nearest neighbor interactions, two of which are intra-chain (V_s') and four which are inter-chain (U_s). For the $|p\rangle$ and $|\ell\rangle$ orbitals (i.e. p-like states) the interactions are a bit more complicated. If we had pure p states in a simple cubic lattice we would only have 4 nearest neighbor interactions as shown in Fig. 3(b). Two of these (types B and D) would have to be zero in this case because of symmetry. For our problem, however, we would need to include all of them. In Fig. 4

we show how the $|p\rangle$ and $|\ell\rangle$ orbitals would look in a simple cubic structure. Some fragments of the infinite chains are identified by the heavy solid lines. The breakdown of the parameters A, B, C and D to intra-chain and inter-chain parameters for the various couplings between $|p\rangle$ and $|\ell\rangle$ orbitals is given in Table I. The usefulness of the simple cubic structure is that we can easily identify all the nearest neighbor interactions and hence the interactions that remain important under a trigonal distortion. The V and U parameters listed in Table I carry through identically in the trigonal structure and are the p-state parameters we use in our "three-dimensional" tight binding model. The fitting of these parameters is <u>not</u> completely arbitrary and can be performed in a very physical way as we shall show in detail later when we present the results of our tight binding models.

IV. Results for Trigonal Phases

A. EPM Results

The simple picture of s-like states, bonding and anti-bonding p-like states and lone-pair states, already confirmed from previous pseudopotential calculations[5-7,14] is well reproduced by our new pseudopotential calculations as shown in Fig. 5(a) for Se and 5(b) for Te. In this figure we display the energy band structure of Se and Te along some high symmetry lines in the hexagonal Brillouin zone together with the corresponding densities of states. A detailed

discussion of the band structures will be given later together with the tight binding results. The density of states spectra were also convoluted with an energy dependent broadening function (1.2 eV for the s-like states and 0.7 eV for the remaining states) in order to facilitate comparison with experiment. This is shown in Fig. 6(a) and 6(b) together with the experimental UPS and XPS measurements of Shevchik et al.[1] for Se and the XPS measurements of Schlüter et al.[2] for Te. All observed structures in the experimental spectra are reproduced within 0.3 eV which is a remarkable improvement over all previous calculations. A very interesting difference between Se and Te appears in the s-like region at energies between -16 eV and -8 eV. Whereas the density of states for Se s-states closely resembles that of a one-dimensional chain (with two singularities at the band-edges), the density of states for the Te s-states looks like a combination of densities of states for a one-dimensional chain and a three-dimensional simple cubic lattice. We see here that the s-states reflect in a very sensitive way the different degrees of anisotropy found in the two crystals. This sensitivity of the s-states to topology also proves to be a very useful tool in interpreting the amorphous spectra of Se and Te, as we shall see in a later section. It is instructive to display the bonding or anti-bonding character of the s-states close to the two band edges. We therefore show in Fig. 7(a) and (b) charge densities for Se obtained

from states at the two band edges. The charge distributions are plotted in a plane containing the shaded area of Fig. 1(a). The bonding and antibonding characteristics are clearly displayed. In the bonding states the charge is almost uniformly concentrated along the chains with small excess charges on each atom, whereas in the anti-bonding states the charge is very strongly concentrated around each individual atom, the wavefunction having a node between neighboring atoms. One notes that the centers of charge do not exactly coincide with the atomic positions; in fact they are displaced towards the central axis of the helices for the bonding states and pushed slightly outside the helices for the anti-bonding states. This asymmetry is compatible with the crystal symmetry, which does not contain spatial inversion. Similar behavior is found for the total charge distribution including all six electrons per atom; here the center of negative charge is displaced towards the center of the helices, thus creating a local static electrical dipole of (0.095 $e^{-}\mathring{A}$) for Se and (0.125 $e^{-}\mathring{A}$) for Te on each atom. These approximate values were obtained by integrating over the charge inside touching spheres centered on each atom. The total dipole moment of course vanishes by summing over the unit cell.

The bonding p-like states whose energies vary between -6 eV and -2.2 eV reveal a very characteristic two-peak structure (see Fig. 6(a) and 6(b)), which is intimately related to two distinct types of bonding states. To understand

the origin of the characteristic two-peak structure we have calculated the electronic charge distributions of states in each peak. This entails summing in equation (7) over states whose energies (in eV) fall within [-6.0, -3.6] and [-3.6, -2.25] for Se and [-6.0, -3.5] and [-3.5, -2.2] for Te. The resulting charge density contour plots are shown in Figs. 8(a) to (d). We find the result, that the lower energy peak in the p-like bonding states corresponds to states which are almost exclusively involved in intra-chain bonding. The charge is well localized in the bonds between neighboring atoms belonging to the same chain. There is no important charge accumulation found between the chains. The upper or higher energy peak contains states which in part arise from a mixing of p_x and p_y functions due to a bond angle $\neq 90°$. However, the charge concentrations in the right hand parts of Figs. 8(b) and (d) are as we shall see direct consequences of inter-chain bonding and might thus be viewed as bonding charges. The pure intra-chain bonding states lie lower in energy than the states contributing to inter-chain bonding since the potential is strongest between neighboring atoms within a chain. A direct proof of the importance of covalent inter-chain bonding in Se and to a lesser extent in Te was obtained in the following way: we repeated the complete calculations for Se with identical potential parameters and identical intra-chain spacings but with an inter-chain distance increased by about 20%. This increase of inter-chain distance

should considerably decrease all inter-chain bonding charges and thus exhibit their importance in the normal trigonal phase. We first discuss some changes in the density of states calculated for this new structure which we shall call Se2. In the s-like region only very small changes towards a more one-dimensional behavior can be recognized. The width of the characteristic two-peak splitting of the bonding p-like states remained unaltered. As we shall see in the discussion of possible amorphous phases this width is sensitive to the bond-angles within the chains. The relative weight of the two peaks in Se2 changed somewhat with respect to Se. The lower energy peak increased, whereas the upper or higher energy peak decreased, thus already indicating a decrease in the inter-chain bonding strength. An equivalent behavior was of course observed for the unoccupied antibonding p-like states. The lone-pair peak remained essentially unaltered with respect to its shape and its position. A very clear picture of the importance of inter-chain bonding in Se can be obtained by comparing the corresponding charge distributions of Se and Se2. In an attempt to focus intention on bonding charges we extracted the short wave length Fourier components of the charge density functions and thus separated out the slowly varying background charge as discussed in Section IIIA. This separation was simply achieved by considering the charge density Fourier series starting at a cutoff wavelength λ_0. For the extraction of bond charges this cutoff was found to

lie naturally at $\lambda_0 = d$ where d is the nearest neighbor distance within the chains of Se. No spurious oscillations in the density distribution occur, if only the positive contributions of the restricted Fourier series to the total charge are considered. The results obtained for Se and Se2 by retaining only Fourier components with $\lambda \leq \lambda_0$ are shown in Figs. 9(a) to (d). By comparing Figs. 9(a) and (c) with the corresponding total charge densities of Se (see Figs. 8(a) and (b)) one can verify the effect of extracting the short wavelength Fourier components in the charge distribution. The most interesting differences between the charge densities of Se and Se2 are found in the higher energy region of the p-like bonding states. The charge pile up in Se in the right hand part of Fig. 9(c) disappears almost completely in Se2 (Fig. 9(d)). This confirms our previous interpretation of this charge contributing to the inter-chain bonding. The decrease of inter-chain bonding in Se2 is coupled to an increase of intra-chain bonding as seen from the rearrangement of charge in Se2 and from the changes in the density of states. We are now in a position to define some measure of intra-chain vs. inter-chain bonding strength in Se and Te by calculating the magnitude of the respective bonding charges. By integrating the charge in Figs. 9(a) and (c) we find for Se 0.07 e^- for the intra-chain bond and 0.04 e^- for the inter-chain bond. It is instructive to compare these values with 0.05 e^- and 0.04 e^- for the intra- and inter-chain

bonding charges of Te respectively. The ratio ξ of intra-chain to inter-chain bonding charge decreases from 1.75 for Se to 1.25 for Te and thus reflects the more three-dimensional or more isotropic character of Te. The smaller amount of total bonding charge in Te is indicative of its more metallic or less covalent character. The absolute values of the charges of course depend strongly on the definition of bonding charges. The indicated values should therefore be considered as a relative measure rather than individually.

B. Tight Binding Results

The tight binding models we have introduced in Section III provide a means of understanding, in a very simple way, the band structures obtained using the more realistic EPM. Certain general features in these band structures (Fig. 5) can be interpreted physically in terms of the type, sign and magnitude of the real space interactions involved.

We begin with the simple tight binding model with only intra-chain parameters. The energy bands (24) to (27) and the associated densities of states (28) to (30) are plotted in Fig. 10. Here we have taken $V_s = -13.0$, $V_s' = -1.3$, $V_p = -.2$, $V_p' = 0$, $V_p'' = 3.8$, $V_p''' = 0.55$, $V_\ell = -1.3$, $V_\ell' = 0.4$, and $V_\ell'' = 0.26$. These parameters are given in units of eV and are shown schematically in Fig. 2. They were fitted to the band structure of Se plotted in Fig. 5. V_s, V_p and V_ℓ represent the center of mass positions of the s-like, p-like-bonding and antibonding, and lone pair states

respectively and were chosen so that the top of the valence band lies at 0 eV. We notice that the overall agreement with the Se band structure and density of states is quite satisfying considering the approximations we are making here. In particular the band structure and density of states of the s-like states of the tight binding model compare surprisingly well with that of Se in Fig. 5. The one-dimensional nature of this region is unmistakable. The one dimensional secant behavior of the density of states is even more prominent in the EPM results of Se2 where the chains are further apart and the inter-chain interaction is greatly reduced. The s-like states of Se using the EPM also show a small asymmetry in the band structure which is perhaps caused by a small s-p interaction that we have ignored in the tight binding case.

The prominent features of the p-like states for Se in Fig. 5 are also reproduced to some extent in Fig. 10. The parameter V_p'' represents interactions between orbitals along the same bond and is responsible for the formation of bonding and antibonding bands. To broaden the bands we could introduce an interaction V_p' between different orbitals on the same atom. However this would put A_3 and Γ_2 lower in energy than A_1 and Γ_3 respectively in the antibonding bands. To obtain the correct ordering, we must include an interaction V_p''' between orbitals on nearest neighbor atoms which are <u>not</u> along the same bond. In addition V_p' must be small.

This is consistent with the fact that the $|p\rangle$ orbitals are very p-like in nature with a rather small hybridization of s and d. For simplicity we take V_p' equal to zero.

The shape of the lone pair bands of Se in the EPM calculation is also reproduced rather well in Fig. 10. To get the correct band ordering at Γ and A it is necessary to include, both first nearest neighbor V_ℓ' and second nearest neighbor V_ℓ'', interactions between $|\ell\rangle$ orbitals. In particular V_ℓ' and V_ℓ'' need to be positive with $V_\ell' > V_\ell''$.

To improve the tight binding Se results and to interpret the EPM Te results it is necessary to introduce inter-chain parameters. This is quite clear from the s-like region of the density of states of Te (Fig. 5) where a "three-dimensional" simple cubic-like density of states structure appears in the middle of the band. The band structures and densities of states of Se and Te using the tight binding model including inter-chain interactions (discussed in Section IIIC) are shown in Fig. 11. The symmetries of the energy levels are assumed to be the same as those for the EPM calculations. We notice that the general agreement between the densities of states and band structures in Fig. 5 and Fig. 11 is rather good. The parameters used in these tight binding calculations are listed in Table II. These parameters are not meant to represent the best fits using this model but rather to give a flavor of the type of interactions involved in reproducing the general features of the more realistic EPM band structures.

Although the $|p\rangle$ and $|\ell\rangle$ interactions seem to be many, they are not physically completely independent and were not adjusted arbitrarily. The method we used to investigate the parameters is rather simple, instructive and conceptually appealing. As we have already mentioned the trigonal structure of Se and particularly Te is rather close to that of a simple cubic structure (Fig. 1). We start therefore with an EPM calculation of simple cubic Te. In the tight binding model we now only have interactions A, B, C and D (Fig. 3(b)) for the p-like functions and $V_s' = U_s$ (Section IIIC) for the s-like functions. Interactions B and D however are now zero because of symmetry. Let us investigate the p-like states first. If we plot the EPM simple cubic band structure along the same symmetry points and lines as in Figs. 5 and 11 we would find at Γ and K a six-fold degenerate and a three-fold degenerate p-like energy level. These levels of course represent the "bonding and lone-pair" states and the "antibonding" states respectively in the trigonal structure. The correct ordering of these levels, in the tight binding model demands that A be positive. From Table I this is equivalent to $V_p'' = U_{\ell p}$ being positive for the simple cubic structure. Furthermore the energy difference between these levels at Γ is smaller than at K. This is intimately related to the smaller energy differences between bonding and lone-pair states and antibonding states at Γ than at K as observed in Fig. 5. To obtain these energy differences

in the simple cubic tight binding model it is necessary to take $C = U_p' = V_{\ell p}'' = U_{\ell p}''$ negative. By fitting these parameters to the EPM simple cubic band structure we get values around $V_p'' = U_{\ell p} \sim +2$ eV and $U_p' = V_{\ell p}'' = U_{\ell p}'' \sim -0.5$ eV.

Let us now break the simple cubic symmetry by introducing a trigonal distortion or equivalently (in the tight binding model) by taking the difference between intra-chain (V) and inter-chain (U) interactions explicitly into account. Physically we would expect the V parameters in general to be larger in magnitude than the U parameters. We first take $V_p'' > U_{\ell p}$. This has the immediate effect of breaking up the "melange" of p-like bands in the simple cubic case into separate p-like bonding, lone-pair, and antibonding bands. These bands form degenerate triplets at Γ, K, H, A and along K to H and A to Γ. In addition these bands form doublets and singlets along Γ to K, H to A and Γ to M to L to A. The general features of these bands are actually already rather similar to those of Se and Te (Fig. 5). In fact the criss-cross character of the lone-pair bands of Te from M to L is also present. If we now take $|V_{\ell p}''| > |U_p'| \neq |U_{\ell p}''|$ nothing very different or new happens. However the relative size of the bonding-antibonding gaps at Γ and K and at H and A are very strongly dependent on the value of U_p'. Since the cubic symmetry is broken interactions B and D are no longer zero. This has some very important consequences for the band structure. We first consider interactions B

(Table I) and take $V_p'''' > U_p \neq 0$. $V_p'''' \neq 0$ creates a broadening or a splitting of the bonding and antibonding triply degenerate levels from K to H and A to Γ. To obtain the correct ordering of the doublet and singlet levels at K, H, A and Γ as shown in Figs. 5 and 11 it is necessary (as in the one-dimensional model) to take V_p'''' positive. The doublet levels along Γ to K and H to A are now no longer degenerate. This degeneracy is also broken with $U_p \neq 0$. In addition U_p has a very strong influence on the relative size of the Γ_2-Γ_3(A_3-A_2) and K_2-K_3(H_3-H_2) gaps of the antibonding (bonding) p-like states. U_p must be taken positive to make Γ_2-Γ_3 and A_3-A_2 bigger than K_2-K_3 and H_3-H_2 respectively as shown in Figs. 5 and 11. The interactions $V_{\ell p}'$ and $U_{\ell p}'$ are also taken to be non-zero, however, they are responsible for only minor changes once $U_{\ell p} \neq 0$.

Let us now examine interactions of type D (Table I). The inclusion of V_p'''' and $U_{\ell p}''''$ causes minor and relatively unimportant changes in the band structures. However $U_p'' \neq 0$ is responsible for a very interesting effect. It is the only parameter that can change the relative size of the Γ_1-Γ_3 and K_1-K_3 gaps of the bonding states and the H_3-H_1 and A_3-A_1 gaps of the antibonding states. To make Γ_1-Γ_3 and A_2-A_1 smaller than K_1-K_3 and H_3-H_1 respectively it is necessary to take U_p'' negative. Finally V_ℓ' and V_ℓ'' produce the same effects as in the one-dimensional calculation. V_ℓ' broadens out the lone-pair bands between A and Γ, and between Γ and K.

Positive values of V_ℓ' and V_ℓ'' are necessary to give the correct bond ordering and to make A_3-A_2 smaller than Γ_2-Γ_3 respectively. U_ℓ has been neglected in general but causes the same effects as V_ℓ'. The only major difference between them is that they have opposite effects on the relative size of the K_2-K_3 and H_3-H_2 gaps of the lone-pair bands.

For the s-like states everything is much simpler. Fitting V_s' and U_s to the simple cubic band structure we get $V_s' = U_s \sim -0.5$. By taking $|V_s'| > |U_s|$ we get all the correct dispersions and band orderings. As we have already mentioned the small asymmetry observed in the s-like region of the Te and Se band structures using the EPM is possibly caused by a small s-p interaction which has been ignored in the tight binding models. We should emphasize again that the s-like states are a very useful and convenient system to study because of their sensitivity to topology and their simplicity. The differences in anisotropy of Se and Te are clearly and unambiguously demonstrated by just comparing the values V_s' and U_s for Se with those of V_s' and U_s for Te. As seen from Table II Se is definitely more anisotropic. This is also revealed in general by comparing the appropriate V and U parameters of Se with those of Te for the p-like functions as shown in Table II.

V. Results for Amorphous Phases

The electronic properties of the amorphous phases of We and Te have been studied in several papers.[7] The results

of theoretical models have usually been compared to experimental optical measurements. Such comparisons are relatively difficult and no conclusive results in particular concerning the structural nature of the amorphous phases could be obtained. With the advent of new XPS and UPS measurements[1,2] important direct information about all the valence bands became available. Moreover, since these measurements were carried out on both crystalline and amorphous phases, a comparative study becomes possible. To explain the differences between the crystalline and amorphous spectra we first tried in the preceding paragraph to understand the origins of the various structures in the crystalline spectrum. We repeat here the main results of this study: 1) The s-like states, which energetically are well separated from the higher p-like states, display in a very sensitive way the more one-dimensional character of Se as compared to Te. 2) The characteristic two-peak structure of the p-like bonding states of both Se and Te is intimately related to two distinct types of bonding states. The splitting is related to the amount of mixing and the relative strength of the two peaks reflects the relative amount of intra- and inter-chain bonding. Specifically, the lower energy peak contains almost exclusively intra-chain bonding states while the upper or higher energy peak contains states forming the inter-chain bonding.

Let us now carefully examine the characteristic changes occurring in the amorphous phase. We thus show in Fig. 12 (top)

the photoemission results of Shevchik et al.[1] for trigonal and amorphous Se. The samples were prepared by dc sputtering in an argon atmosphere. The trigonal crystalline phase was obtained by subsequent annealing. The overall structure of the trigonal and amorphous spectra remains essentially unaltered. In particular no broadening with respect to the crystalline phase can be observed in the amorphous phase. This experimental fact is in disagreement with the theoretical model developed by Kramer and co-workers[7] which is based on short-range order and a specific form of long-range disorder and which gives rise to broadening effects.

In the lone-pair region (between -2 eV and 0 eV) the amorphous spectrum has lost some fine-structure and perhaps is shifted slightly to higher energies. We may conclude from this that the non-bonding p-states remain essentially unaltered in the amorphous phase and do not hybridize noticeably. However, in the bonding p-like region (between -6 eV and -2 eV) very interesting changes have occurred. The lower energy peak has become weaker whereas the higher energy peak increased in the amorphous phase. On the basis of our analysis of the crystalline case we suggest that this reversal corresponds to a decrease of the number of pure intra-chain bonding states. As a consequence there are now more electrons occupying states which are partially localized outside the chains. By performing several model calculations of trigonal phases of Se with various bond angles (the nearest intra-

and inter-chain distances were kept constant) we found that the splitting in the bonding p-like states is very sensitive to bond angle variations and hence to the mixing. In particular we found that for chains with 90° bond angles the splitting disappeared because of the equivalence of the two different p-states. For bond angles $\gtrsim$ 120° the splitting also decreased due to an increase in interaction with the lone-pair states. In the amorphous phase, however, this splitting remains essentially unchanged thus suggesting that bond angle variations are relatively small.

A very unusual effect appears in the s-like region (between -18 eV and -7 eV) of Se. The dip in the photo-emission curve seems to be deeper in the amorphous phase than in the crystalline phase. Since we know that the density of s-like states is very sensitive to topology, this effect indicates some very interesting structural properties. For example it could not be caused by just a breaking of the infinite chains, since this would rather tend to fill up the dip in the density of states, unless the broken chains were of order two which seems rather unlikely because of the preference of Se for two fold coordination. A reasonable explanation of the increase of the dip, however is the formation of some type of rings. In particular the dip would increase if the rings were of order three, five, six or seven. Rings of order four, eight, or five and seven together, would certainly tend to fill up the dip in the density of states.[15]

Furthermore, since the bond angles in the trigonal phase are about 104° and since bond-angle variations seem to be small, the most likely ring structures would be of type five-fold and six-fold, or six-fold and seven-fold. To demonstrate the effect of the existence of rings on the density of states, we have carried out two different model calculations on Se containing only six-fold and only eight-fold rings respectively. The rings were arranged in layer-like configurations to that bond-angles, nearest neighbor distances and second nearest neighbor distances were identical to those in the trigonal form. The resulting densities of states are shown in Fig. 13. We notice that the structure in the s-like region behaves essentially as expected for isolated rings. The six-fold ring configuration gives rise to a pronounced dip in the density of states around -13 eV while the eight-fold ring structure gives a peak. In the p-like bonding region we essentially obtain the same results as in the experimental amorphous spectrum, i.e. a shift of strength to higher energies. It is not clear, however, whether this shift is a consequence of ring resonances or of the different inter-ring environment.

On the basis of this analysis we propose that the amorphous Se sample used in the photoemission measurements of Shevchik et al.[1] contains a substantial number of atoms in ring-like configurations of order six, five and maybe seven. This suggestion seems to be consistent with Rechtin and Avenbachs[16] interpretation of their radial distribution

function data. The existence of a substantial number of eight-fold rings, as often proposed for amorphous Se,[1] seems to be a rather questionable possible structural feature for this sample.

The photoemission results for crystalline and amorphous Te obtained by Shevchik et al.[1] using the same sputtering technique as for their Te sample give similar results. However, these results differ considerably from photoemission data on amorphous Te prepared by argon bombardment.[2] The latter results are shown in Fig. 12 (bottom) together with the crystalline spectrum obtained on the same sample before argon bombardment. As in Se the lone-pair regions remain relatively unaltered. In the bonding p-like region (between -6 eV and -2 eV) we find in contrast to Se a shift of strength to lower energies. This suggests an increase in the number of pure intra-chain bonding states, which is consistent with an increase of covalency of Te in the amorphous phase. The structural information derived from the density of states in the s-like region is somewhat more difficult to discern since there now seems to be a filling up of the dip in the amorphous case. As mentioned, a filling up can be obtained in various ways, such as regions of simple cubic short range order, four-fold, eight-fold, five- and seven-fold ring configurations and broken chains. In spite of the fact that the structure of trigonal Te is close to the simple cubic structure, regions of simple cubic structure can be dismissed, since these would

give rise to a merging of the p-like bonding states with the lone-pair states. What remains therefore, is to discern between structures which contain mostly broken chains or broken chains with a substantial amount of rings. It is however rather difficult to make a conclusive statement about the structure of this sample of amorphous Te without better experimental resolution. For instance it is not really clear that the two peaks in the p-like bonding states have not merged in the amorphous phase. One could speculate, however, that argon bombardment tends to leave the system with atoms existing mostly in broken chain configurations. On the other hand sputtering and the deposition of thin films may favor the formation of rings.

VI. Summary and Conclusions

We have presented a detailed study of the density of states of trigonal Se and Te. This was accomplished by first performing new EPM calculations which give an excellent fit to recent photoemission measurements.[1-3] This enabled us to perform charge density calculations which were obtained as a function of energy and evaluated within specific energy intervals associated with corresponding specific peaks in the density of states. In particular the characteristic two-peak structure in the bonding p-like states is interpreted as involving intra-chain bonding (lower energy peak) and inter-chain bonding (higher energy peak) states. This interpretation is confirmed by pulling the chains apart and

finding that the localized charge between the chains is greatly reduced while the lone-pairs, etc. remain relatively unchanged. Thus this type of "bonding" must be added to the usual van der Waals interaction to obtain the total interaction between the chains. In addition we have calculated the amount of s and d character in the p-like region. We find in general a presence of around 5-10% s and 1-5% d character in the wave-functions. This p-d admixture should be enough to change the bond angle from 90° to 104° without involving a strong s-p admixture. A strong s-p admixture as suggested by Chen[4] to account for the 104° bond angle is not necessary and not supported by the recent photoemission results.[1-3]

We have also introduced a "one-dimensional" and "three-dimensional" tight binding model which includes only intra-chain and intra- and inter-chain interactions respectively. The simplicity of the "one-dimensional" model is exploited by obtaining analytic expressions for the energy bands and associated densities of states. The results show the closely "one-dimensional" or strongly anisotropic nature of Se and the sensitivity of the s-like states to topology. The "three-dimensional" tight binding model is introduced to get a better description of Se and to treat the relatively more isotropic Te. By fitting the band structures of this model to those of Se and Te using the EPM it is easy to identify the most important real space orbital-orbital inter-actions and therefore obtain a physical understanding of the

origins of various features in the band structures.

With a good understanding of the trigonal forms of Se and Te at hand, we have analyzed the changes observed in the photoemission spectra of amorphous Se and Te. In particular there are changes between the trigonal spectra and the amorphous spectra, and differences between the amorphous spectra depending on sample preparation. Specifically argon bombardment and sputtering seem to create two different types of amorphous phases. This is reflected clearly in the s-like region of the spectra. For example in Fig. 12 the s-like region shows a bigger dip in the amorphous phase (sputtering) than in the trigonal phase of Se[1] whereas for Te[2] (argon bombardment) the exact opposite is obtained. This increased dip for amorphous Se (also for Te[1] if obtained by sputtering) can be associated with the presence of five or six fold rings of bonds and tends to reject the presence of eight-fold rings of bonds as often suggested. This was shown in Fig. 13 where we plotted the density of states of two model calculations of Se containing only six- and eight-fold rings respectively. The rings were arranged in layer-like configurations with bond-angles, nearest neighbor distances and second nearest-neighbor distances identical to those in the trigonal form. The s-like region of the amorphous Te sample obtained by argon bombardment[2] is a bit more difficult to interpret. A filling up of the dip could now be caused either by rings (e.g. eight fold) and/or broken chains. It is our

feeling however that argon bombardment may favor the formation of broken chains since here one is essentially perturbing the surface structure of a "perfect" trigonal crystal. Finally the changes observed in the p-like bonding region of Se (sputtered) suggest that there is a decrease in the number of pure intra-chain bonding states for the amorphous phase. As a consequence there are now more electrons occupying states which are partially localized outside the chains. In the case of amorphous Te (argon bombardment) the opposite is true. This would suggest an increase in covalency for this sample of amorphous Te.

References

* Supported in part by the National Science Foundation and the U.S. Atomic Energy Commission

† Present address: Department of Physics, MIT, Cambridge, Mass.

‡ Swiss National Science Foundation postdoctoral fellow.

1. N. J. Shevchik, J. Tejeda, M. Cardona and D. W. Langer, Solid State Comm. 12, 1285 (1973) and N. J. Shevchik, M. Cardona and J. Tejeda, Phys. Rev. B8, 2833 (1973).
2. M. Schlüter, J. D. Joannopoulos, M. L. Cohen, L. Ley, S. Kowalczyk, R. Pollak and D. A. Shirley, to be published.
3. T. Ichikawa, J. Phys. Soc. Japan 36, 1213 (1974).
4. S. Tutihasi and I. Chen, Phys. Rev. 158, 623 (1967) and I. Chen, Phys. Rev. B7, 3672 (1973).
5. R. Sandrock, Phys. Rev. 169, 642 (1968).
6. K. Maschke, phys. status solidi, b47, 511 (1971).
7. B. Kramer, K. Maschke and L. D. Lande, Phys. Rev. B8, 578 (1973) and references therein.
8. M. L. Cohen and V. Heine, in Solid State Physics, edited by H. Ehrenreich, F. Seitz and D. Turnbull (Academic Press, New York, 1970), vol. 24, p. 37.
9. F. Hulliger and E. Mooser, in Progress in Solid State Chemistry (Pergamon Press, Oxford, 1965) vol. 2, p. 330.
10. J. Stuke, in The Physics of Se and Te, ed. by W. C. Cooper (Pergamon Press, Oxford, 1969), p. 3.
11. P. Löwdin, J. Chem. Phys. 19, 1396 (1951).

12. G. Gilat and L. J. Raubenheimer, Phys. Rev. 144, 390 (1966).

13. M. F. Thorpe and D. Weaire, Phys. Rev. B4, 3518 (1971).

14. M. Schüter, Int. J. of Quant. Chem. 7, 527 (1973).

15. J. D. Joannopoulos, F. Yndurain, L. Falicov and M. L. Cohen, IBM International Topical Conference on Tetrahedrally Bonded Amorphous Solids, (in press).

16. M. D. Rechtin and B. L. Averbach, Solid State Comm. 13, 491 (1973).

Table Captions

Table I. Interactions between p-like states on different atoms. The first column gives the type of interactions as shown in Fig. 3(b), the second column designates the type of orbitals involved, and the third column gives the total number of interactions per atom. The third and fourth columns give the number of interactions, an example of the specific orbitals involved (see Fig. 4), and the parameter used to designate the interactions for intra-chain and interchain coupling respectively. All intra-chain and inter-chain parameters are labelled V and U respectively.

Table II. Interactions and parameters used in the tight binding model including intra-chain (V) and inter-chain (U) interactions for Se and Te. The parameters are defined in the text and are given in units of eV.

Table I

TYPE	INTERACTIONS	TOTAL	INTRA CHAIN	INTER CHAIN
A	$\langle p\|H\|p\rangle$	2	2 (1|2) V_p''	
	$\langle \ell\|H\|p\rangle$	4		4 (1|8) $U_{\ell p}$
B	$\langle p\|H\|p\rangle$	12	4 (1|3) V_p'''	8 (1|5) U_p
	$\langle \ell\|H\|p\rangle$	8	4 (1|9) $V'_{\ell p}$	4 (4|8) $U'_{\ell p}$
	$\langle \ell\|H\|\ell\rangle$	4		4 (7|8) U_ℓ
C	$\langle p\|H\|p\rangle$	4		4 (4|5) U_p'
	$\langle \ell\|H\|p\rangle$	8	4 (4|9) $V''_{\ell p}$	4 (7|6) $U''_{\ell p}$
D	$\langle p\|H\|p\rangle$	6	2 (4|3) V_p''''	4 (4|6) U_p''
	$\langle \ell\|H\|p\rangle$	4		4 (7|5) $U'''_{\ell p}$
	$\langle \ell\|H\|p\rangle$	2	2 (7|9) V_ℓ'	

Table II

TYPE	Se	Te
V_s	-13.1	-10.6
V_s'	-1.1	-0.7
U_s	-0.1	-0.25
V_p	-0.2	-1.0
V_p'	0	0
V_p''	3.4	2.2
$U_{\ell p}$	0.7	1.0
V_p'''	0.4	0.2
U_p	0.2	0.15
$V_{\ell p}'$	0.2	0.2
$U_{\ell p}'$	0.1	-0.1
U_p'	-0.05	-0.2
$V_{\ell p}''$	-0.7	-0.7
$U_{\ell p}''$	-0.3	-0.4
V_p''''	0	-0.1
U_p''	-0.3	-0.25
$U_{\ell p}'''$	-0.1	0.1
V_ℓ	-1.0	-1.2
V_ℓ'	0.2	0.2
V_ℓ''	0.1	0.1
U_ℓ	0	0

Figure Captions

Fig. 1.(a) Unit cell of trigonal Se and Te. The plane in which charge densities are represented is indicated as a shaded area.

(b) The corresponding simple cubic unit structure from which the structure of Se and Te can be derived by trigonal distortions.

Fig. 2.(a) A schematic representation of the s-like ($|s\rangle$), lone-pair ($|\ell\rangle$), and mixed and hybridized p-like functions ($|p\rangle$) used in the tight binding models.

(b) A sketch of the respective orbitals along a chain from Fig. 1(a) and the interactions used for the tight binding model including only intra-chain interactions.

Fig. 3.(a) A sketch of $|p\rangle$ orbitals along a chain with a reference atom i. The letters a_1, a_2, b_1, b_2 etc. represent the coefficients of each $|p\rangle$ orbital in the expansion of the total wave function of the system.

(b) The possible nearest neighbor interactions of p-functions in a simple cubic lattice.

Fig. 4. The arrangement of $|p\rangle$ and $|\ell\rangle$ orbitals in a simple cubic lattice. The heavy solid lines identify the chains as they would exist in the trigonal structure. A few of the orbitals are labelled to identify the $\langle p|H|p\rangle$, $\langle \ell|H|p\rangle$ and $\langle \ell|H|\ell\rangle$ interactions as used in the tight binding model including intra- and inter-chain couplings. These interaction parameters are listed in Table I.

Fig. 5. EPM band structure of trigonal Se (a) and Te (b) along some high symmetry lines in the hexagonal Brillouin zone. The corresponding densities of states are also given.

Fig. 6. Calculated densities of states (solid lines) for trigonal Se (a) and Te (b), which for comparison have been broadened by 1.2 eV for the s-like states and by 0.7 eV for the remaining states. Superimposed are the experimental photoemission spectra (dashed lines) for Se and Te as obtained from refs. 1 and 2 respectively. The scales for the XPS and UPS curves are arbitrary.

Fig. 7. Calculated charge density for states (a) at the bottom of the s-like band and (b) at the top of the s-like band of trigonal Se. The units are arbitrary and are only to be used for comparison.

Fig. 8. Calculated charge densities for Se (a) and (b) and Te (c) and (d) for the lower (a) and (c) and upper (b) and (d) p-like bonding states. The energy intervals are indicated. The values are in units of e/Ω.

Fig. 9. Bonding charges of trigonal Se (a) and (c) and of a model structure of Se (b) and (d) in which the inter-chain distance has been increased by 20%. The charges have been calculated for the lower (a) and (b) and upper (c) and (d) p-like bonding states, retaining only short wavelength components as described in the text. Only positive contours are shown, with values in units of e/Ω.

Fig. 10. Density of states[a] and band structure[b] obtained using the tight binding model including only intra-chain interactions. The parameters of this "one-dimensional" tight binding model are discussed in the text.

Fig. 11. Densities of states and corresponding band structures for Se (a) and Te (b) as obtained from the tight binding model including intra- and inter-chain parameters. The parameters of this "three-dimensional" model are discussed in the text with their values listed in Table II.

Fig. 12. X-ray and ultraviolet photoemission results (top) on trigonal (solid line) and amorphous (dashed line) Se as obtained from ref. 1. X-ray photoemission results (bottom) on trigonal (solid line) and amorphous (dashed line) Te as obtained from ref. 2.

Fig. 13. Density of states of Se in model structures containing only six-fold (solid line) and only eight-fold (dashed line) rings of atoms as obtained from EPM calculations. The curves are broadened as in Fig. 6.

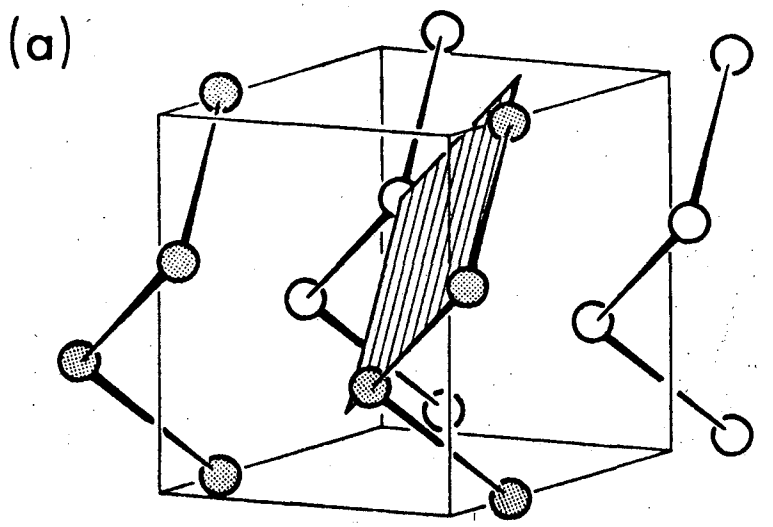

TRIGONAL

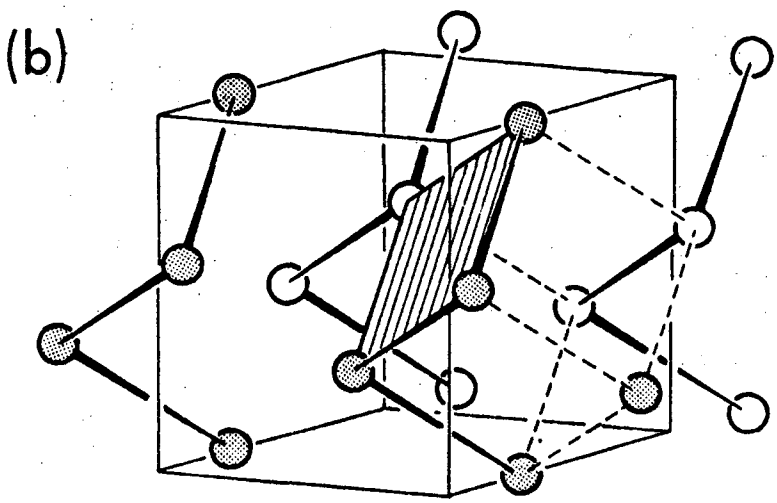

CUBIC

Fig. 1

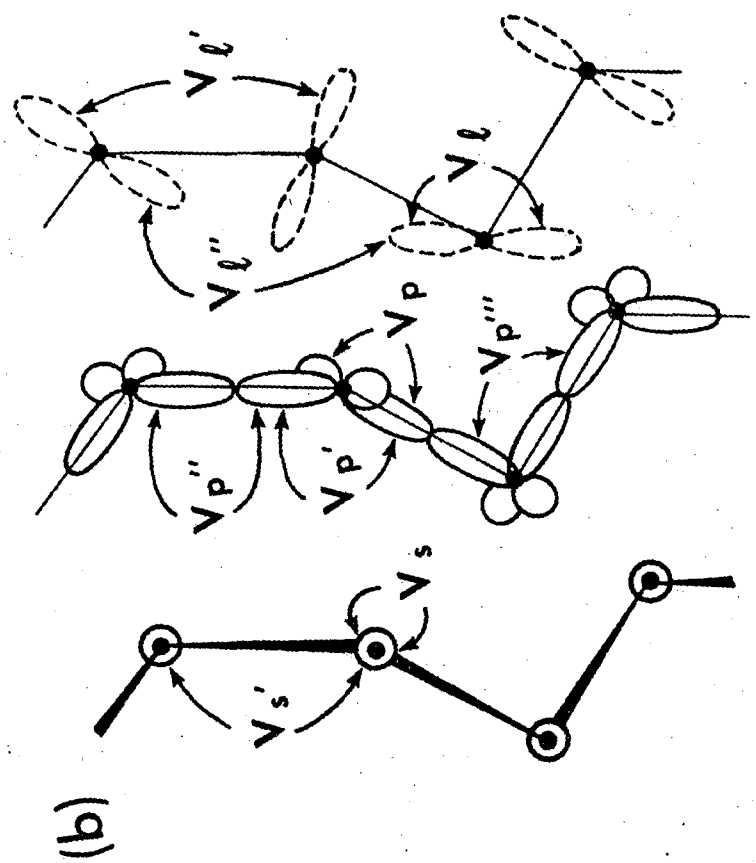

Fig. 2

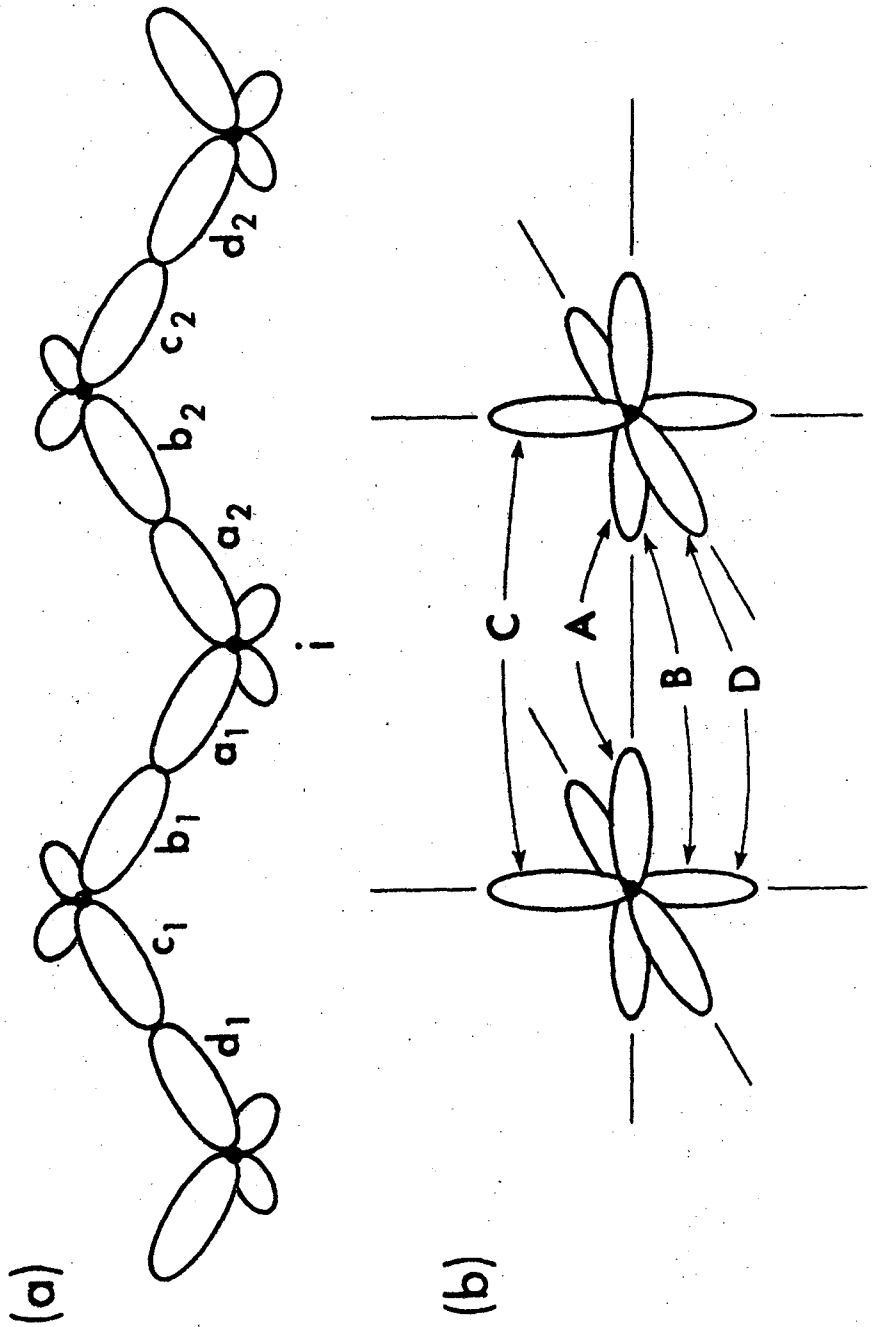

Fig. 3

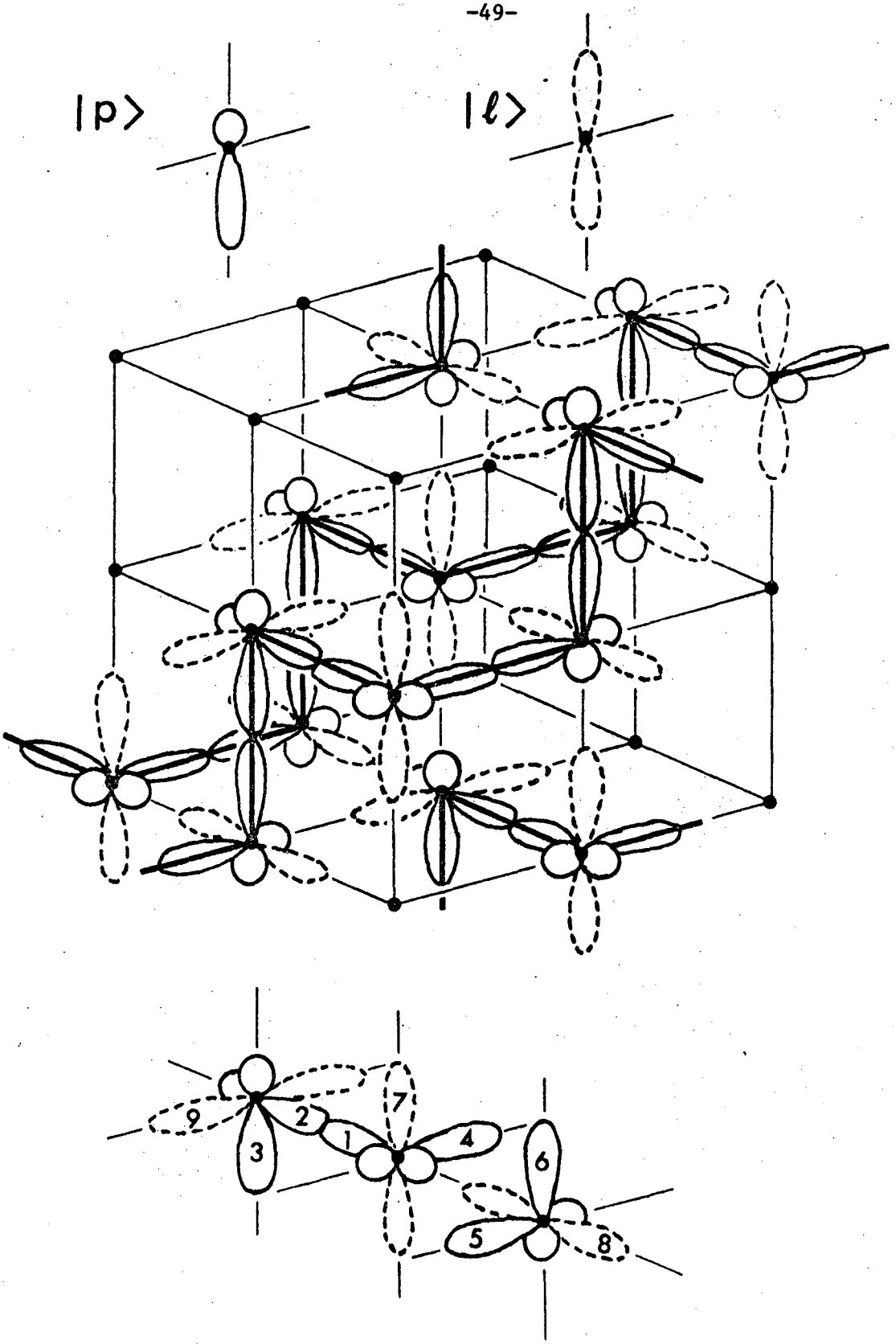

Fig. 4

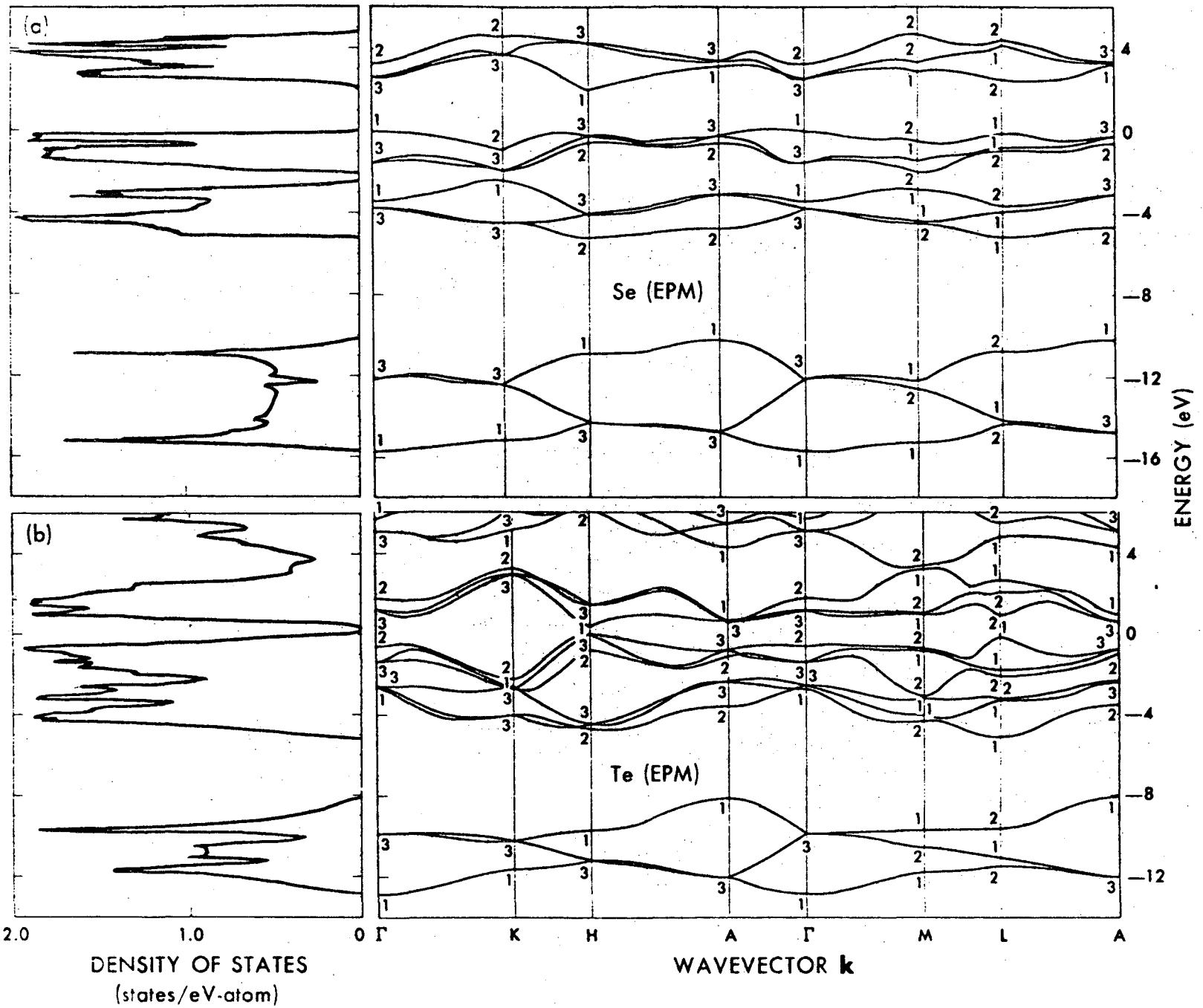
(a)
(b)
Se (EPM)
Te (EPM)
4
0
−4
−8
−12
−16
ENERGY (eV)
2.0
1.0
0
DENSITY OF STATES
(states/eV-atom)
Γ
K
H
A
Γ
M
L
A
WAVEVECTOR k

Fig. 5

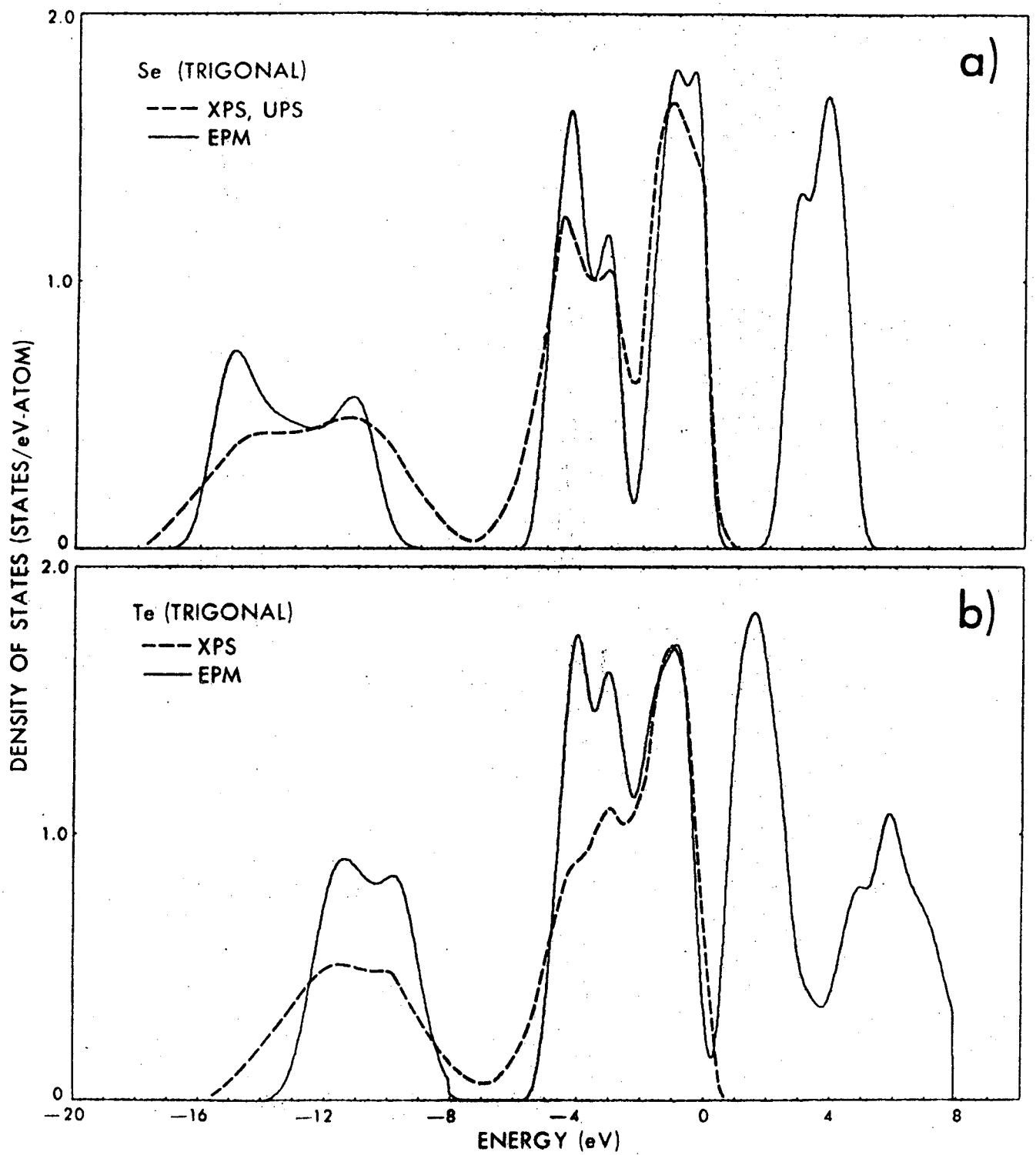
Se (TRIGONAL)
XPS, UPS
EPM
a)
Te (TRIGONAL)
XPS
EPM
b)
DENSITY OF STATES (STATES/eV-ATOM)
2.0
1.0
0
−20
−16
−12
−8
−4
0
4
8
ENERGY (eV)

Fig. 6

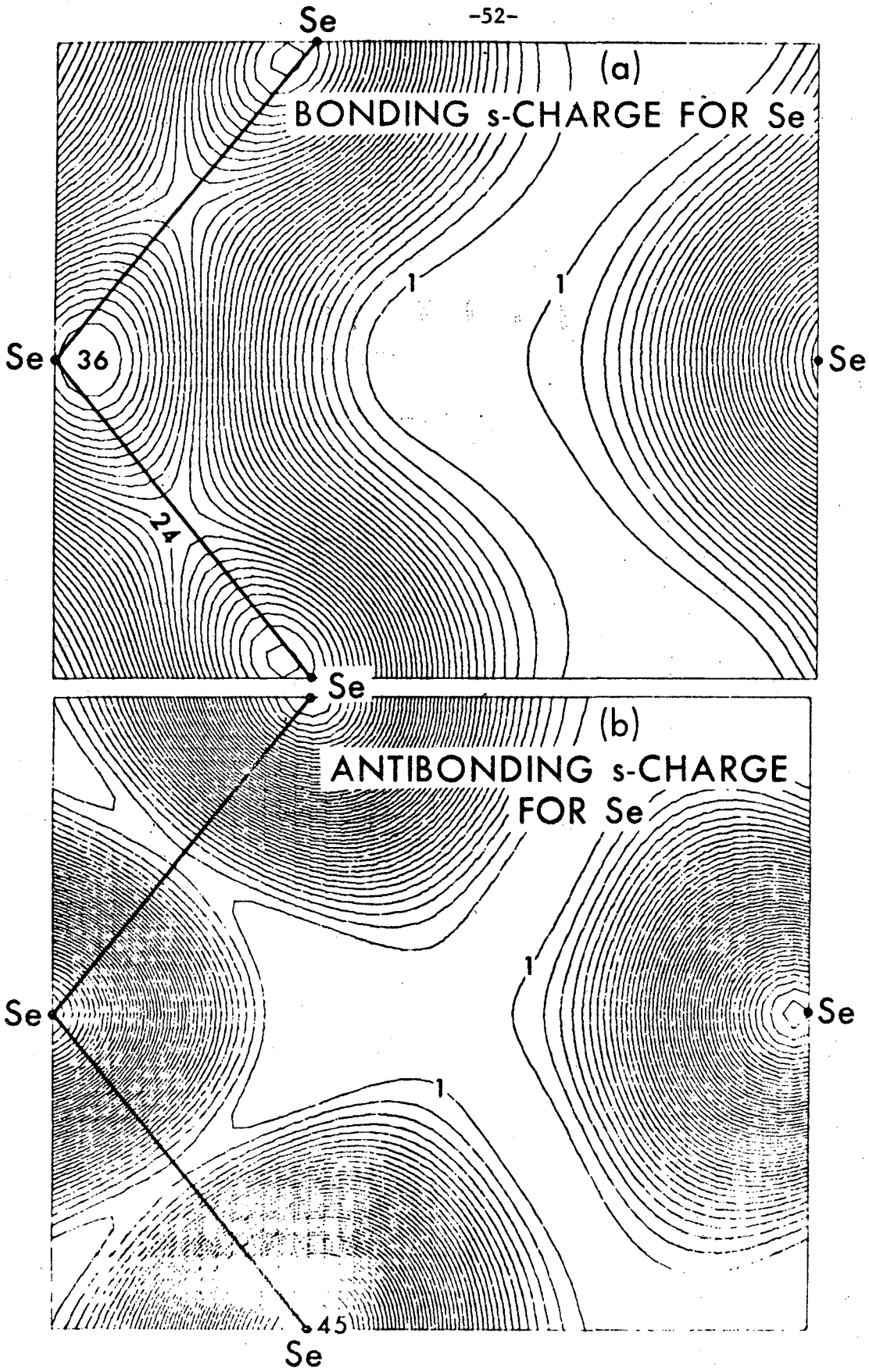
Se
(a)
BONDING s-CHARGE FOR Se
1
1
Se
36
Se
24
Se
(b)
ANTIBONDING s-CHARGE
FOR Se
1
Se
Se
1
45
Se

Fig. 7

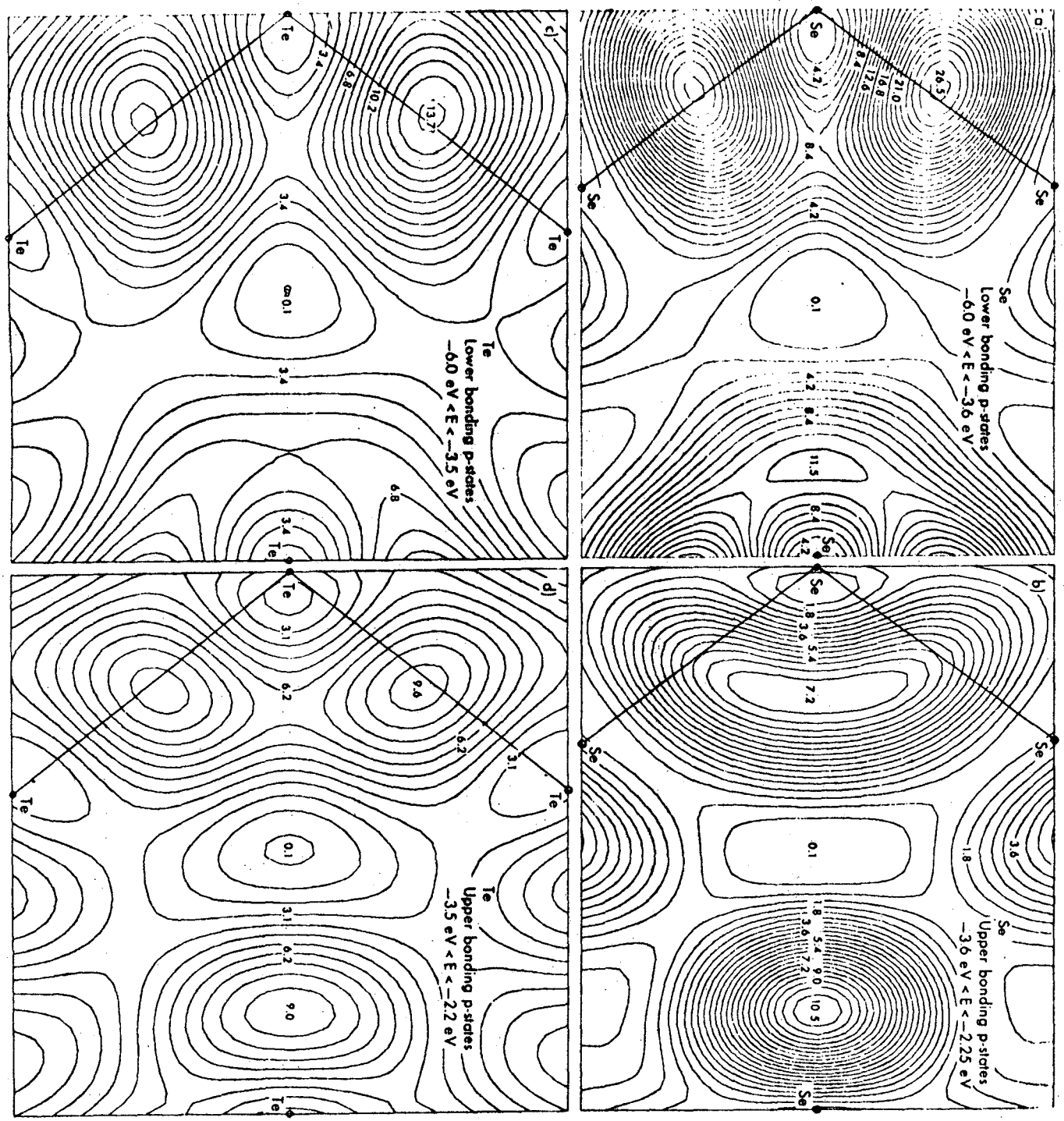
a)
Lower bonding p-states
−6.0 eV < E < −3.6 eV
Se
b)
Upper bonding p-states
−3.6 eV < E < −2.25 eV
Se
c)
Lower bonding p-states
−6.0 eV < E < −3.5 eV
Te
d)
Upper bonding p-states
−3.5 eV < E < −2.2 eV
Te

Fig. 8

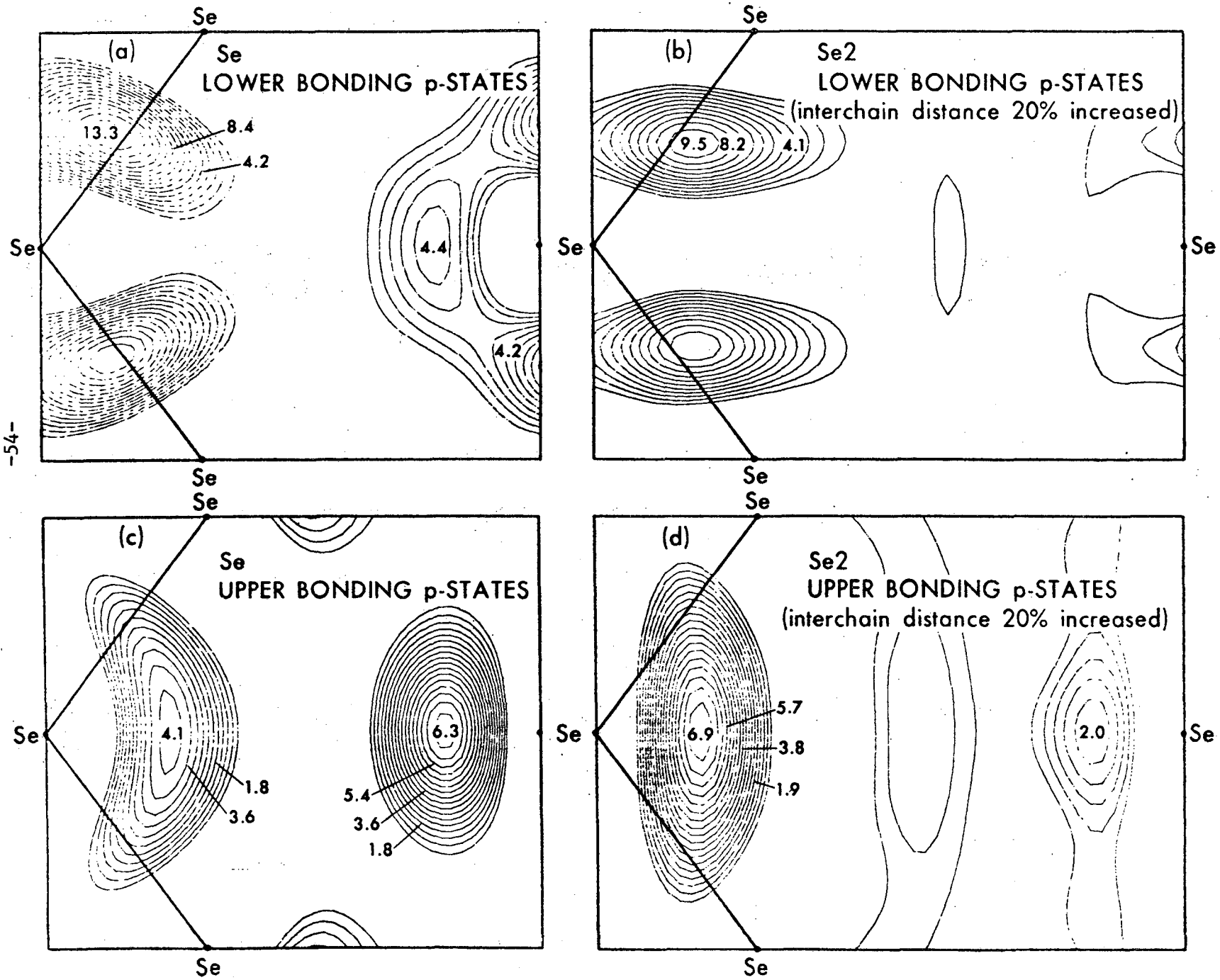
(a)
Se
LOWER BONDING p-STATES
13.3
8.4
4.2
4.4
4.2
Se
Se
Se
(b)
Se2
LOWER BONDING p-STATES
(interchain distance 20% increased)
9.5
8.2
4.1
Se
Se
Se
(c)
Se
UPPER BONDING p-STATES
4.1
1.8
3.6
6.3
5.4
3.6
1.8
Se
Se
Se
(d)
Se2
UPPER BONDING p-STATES
(interchain distance 20% increased)
6.9
5.7
3.8
1.9
2.0
Se
Se
Se

Fig. 9

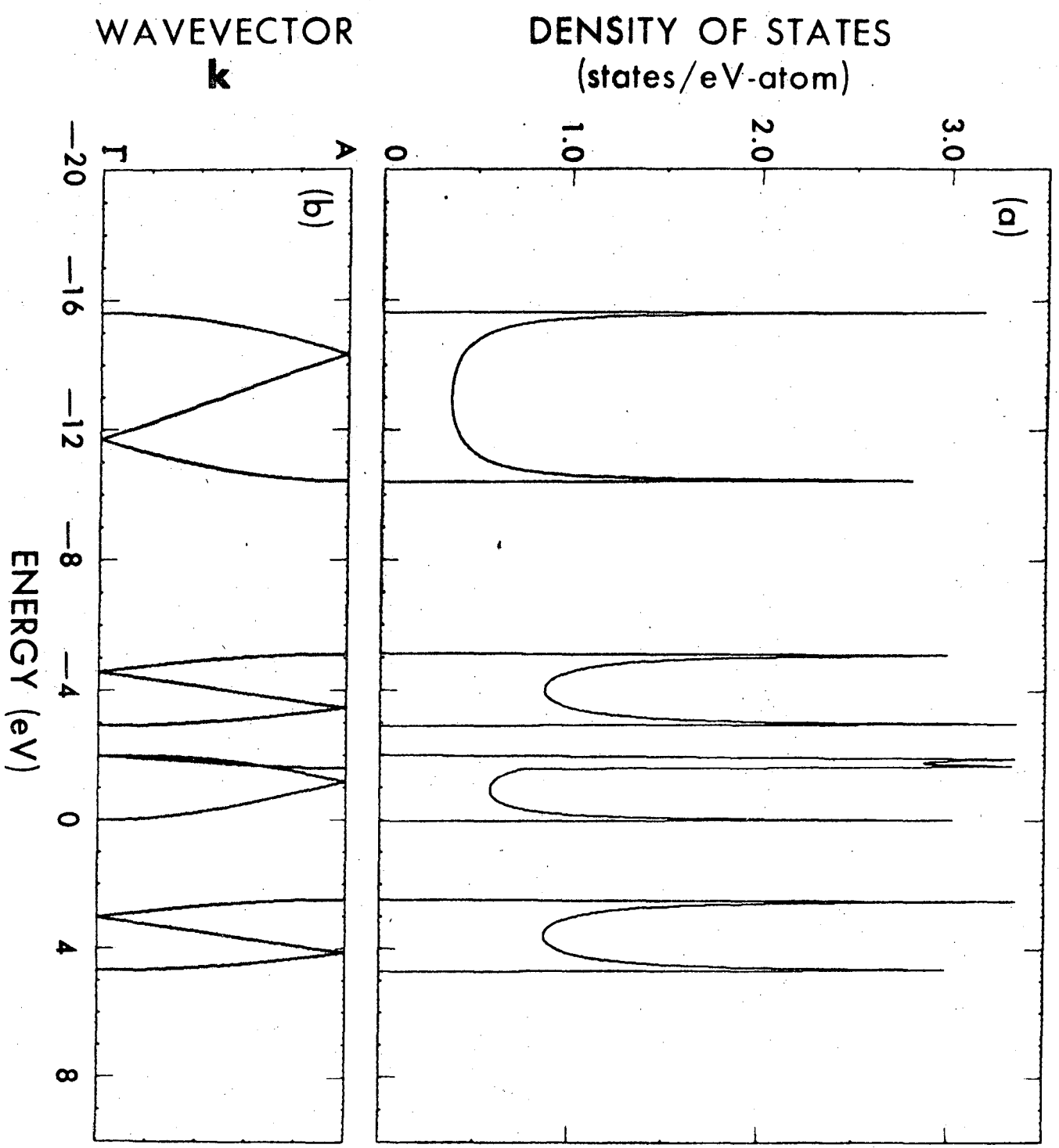
WAVEVECTOR
k
DENSITY OF STATES
(states/eV-atom)
Γ
A
(b)
(a)
ENERGY (eV)
−20
−16
−12
−8
−4
0
4
8
0
1.0
2.0
3.0

Fig. 10

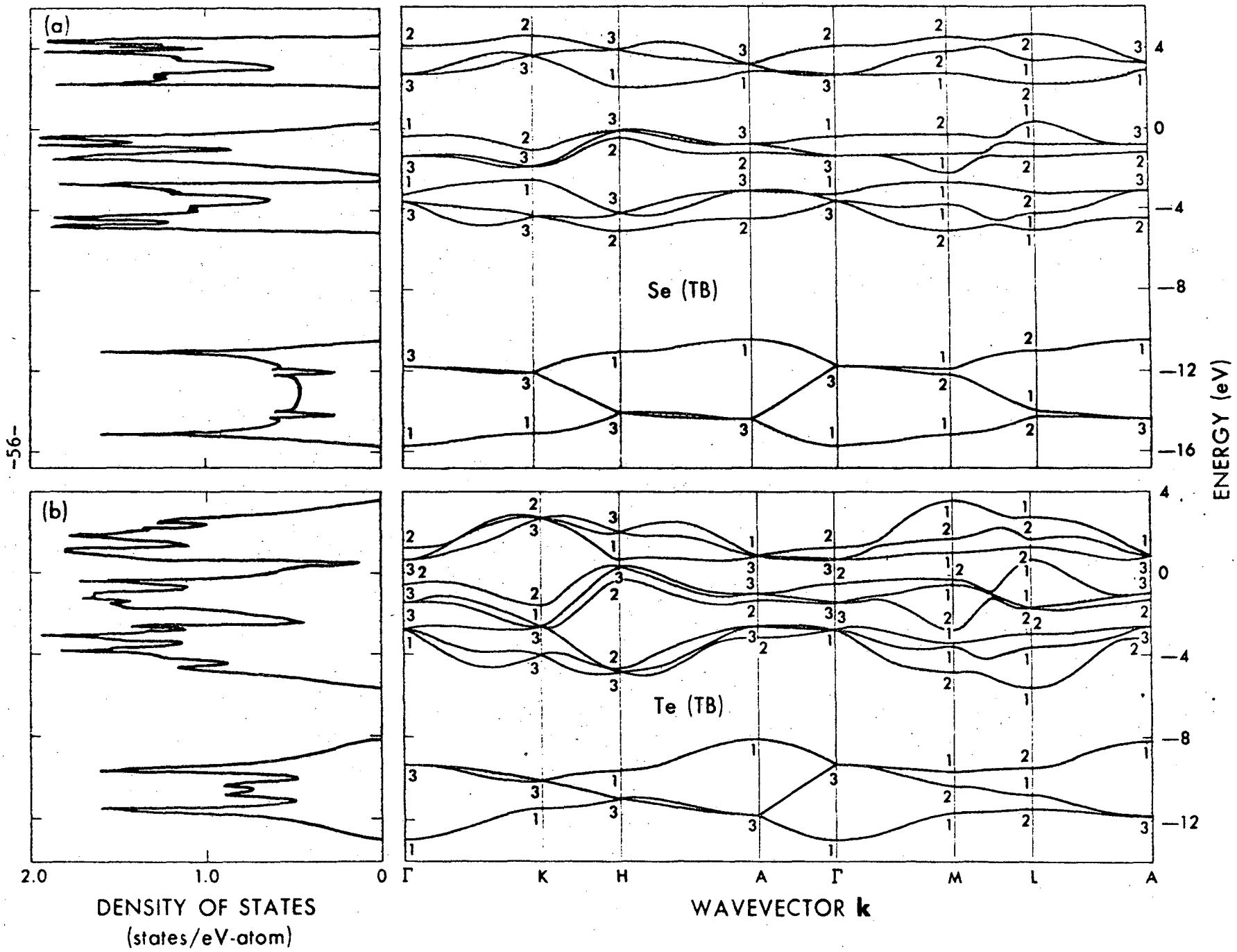
(a)
(b)
Se (TB)
Te (TB)
4
0
−4
−8
−12
−16
ENERGY (eV)
2.0
1.0
0
DENSITY OF STATES
(states/eV-atom)
Γ
K
H
A
Γ
M
L
A
WAVEVECTOR k

Fig. 11

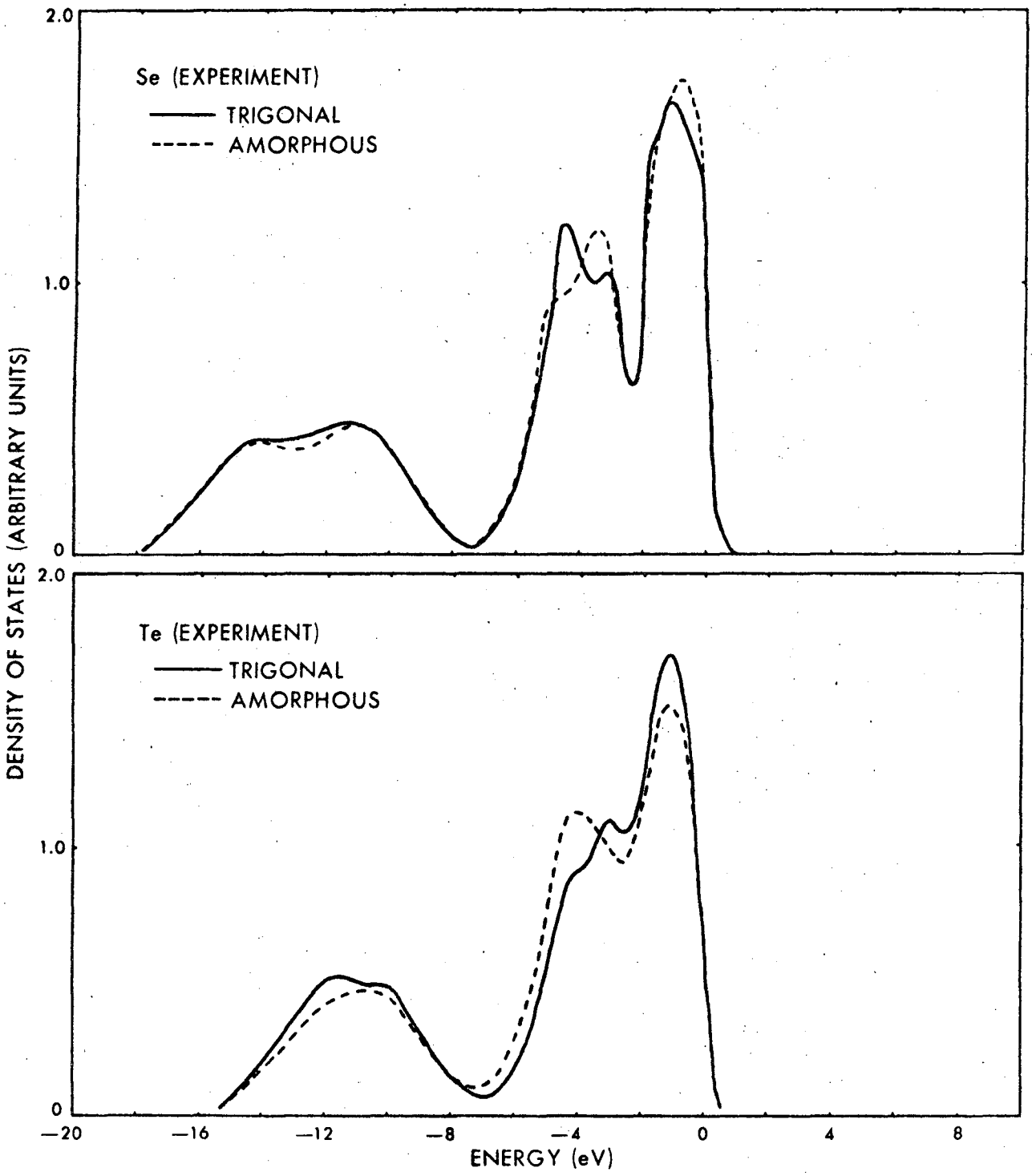
Se (EXPERIMENT)
TRIGONAL
AMORPHOUS
Te (EXPERIMENT)
TRIGONAL
AMORPHOUS
DENSITY OF STATES (ARBITRARY UNITS)
2.0
1.0
0
−20
−16
−12
−8
−4
0
4
8
ENERGY (eV)

Fig. 12

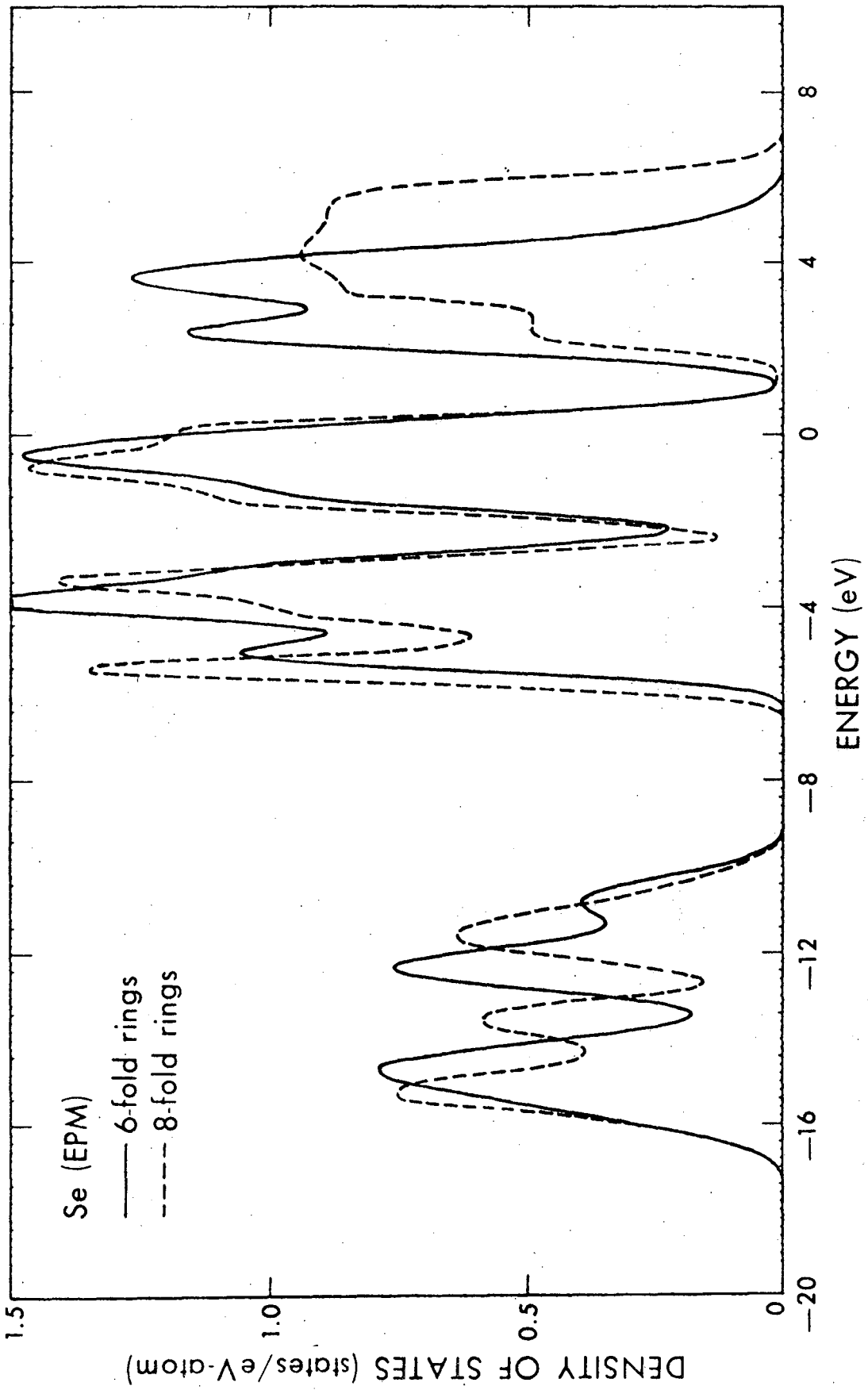
Se (EPM)
6-fold rings
8-fold rings
DENSITY OF STATES (states/eV-atom)
ENERGY (eV)
1.5
1.0
0.5
0
8
4
0
−4
−8
−12
−16
−20

Fig. 13

TECHNICAL INFORMATION DIVISION
LAWRENCE BERKELEY LABORATORY
UNIVERSITY OF CALIFORNIA
BERKELEY, CALIFORNIA 94720